J Neurophysiol 98: 638–656, 2007.
First published May 30, 2007; doi:10.1152/jn.00382.2007.

Differential Expression of Intrinsic Membrane Currents in Defined Cell Types of the Anterolateral Bed Nucleus of the Stria Terminalis

Sayamwong E. Hammack, Irakli Mania, and Donald G. Rainnie
Department of Psychiatry and Behavioral Science, Center for Behavioral Neuroscience, Emory University, Atlanta, Georgia

Submitted 3 April 2007; accepted in final form 28 May 2007

Hammack SE, Mania I, Rainnie DG. Differential expression of intrinsic membrane currents in defined cell types of the anterolateral bed nucleus of the stria terminalis. *J Neurophysiol* 98: 638–656, 2007. First published May 30, 2007; doi:10.1152/jn.00382.2007. The anterolateral group of the bed nucleus of the stria terminalis ($BNST_{ALG}$) plays a critical role in a diverse array of behaviors, although little is known of the physiological properties of neurons in this region. Using whole cell patch-clamp recordings from rat $BNST_{ALG}$ slices in vitro, we describe three distinct physiological cell types. Type I neurons were characterized by the presence of a depolarizing sag in response to hyperpolarizing current injection that resembled activation of the hyperpolarization-activated cation current I_h and a regular firing pattern in response to depolarizing current injection. Type II neurons exhibited the same depolarizing sag in response to hyperpolarizing current injection, but burst-fired in response to depolarizing current injection, which was indicative of the activation of the low-threshold calcium current I_T. Type III neurons did not exhibit a depolarizing sag in response to hyperpolarizing current injection, but instead exhibited a fast time-independent rectification that became more pronounced with increased amplitude of hyperpolarizing current injection, and was indicative of activation of the inwardly rectifying potassium current $I_{K(IR)}$. Type III neurons also exhibited a regular firing pattern in response to depolarizing current. Using voltage-clamp analysis we further characterized the primary active currents that shaped the physiological properties of these distinct cell types, including I_h, I_T, $I_{K(IR)}$, the voltage-dependent potassium current I_A, and the persistent sodium current I_{NaP}. The functional relevance of each cell type is discussed in relation to prior anatomical studies, as well as how these currents may interact to modulate neuronal activity within the $BNST_{ALG}$.

INTRODUCTION

A growing body of evidence suggests that the modulation of neural activity in the bed nucleus of the stria terminalis (BNST) plays a critical role in the expression of a diverse array of behaviors, such as anxiety-like behavior (Walker et al. 2003), learned helplessness (Hammack et al. 2004), drug reinforcement (for review, see Aston-Jones and Harris 2004), drug reinstatement behavior (Erb and Stewart 1999), conditioned defeat (Jasnow et al. 2004), and circadian rhythmicity (Amir et al. 2004). This diversity suggests an underlying BNST neurocircuitry that might be equally varied.

Indeed, the BNST is a complex structure that can be grossly divided not only into anterior and posterior subdivisions by the fibers of the stria terminalis (De Olmos et al. 1985; Ju et al. 1989), but also into dorsal and ventral subdivisions by the fibers of the anterior commissure (De Olmos et al. 1985; Ju et al. 1989). However, as many as 30 individual subdivisions have been identified in the BNST based on their cytoarchitecture, chemoarchitecture, and connectivity (Dong et al. 2001; Ju et al. 1989), suggesting that functional specificity may also be ascribed to different subregions within the BNST. Consistent with this hypothesis, more medial BNST subregions form an integral part of the medial extended amygdala and are believed to mediate the expression of defense and reproductive behaviors (for review, see Newman 1999). In contrast, the more lateral BNST subdivisions form part of the central extended amygdala (Alheid and Heimer 1988) and mediate the expression of behaviors associated with affect (Walker et al. 2003).

Excitability of the central extended amygdala is tightly regulated by afferent projections arising from the basolateral nucleus of the amygdala (BLA) (Adamec 1989; Casada and Dafny 1992; Dalsass and Siegel 1987; Dong et al. 2001) and, not surprisingly, BLA lesions block many of the same affective behaviors thought to be mediated by activation of the central extended amygdala (Walker and Davis 1997). Significantly, afferent projections from the BLA primarily target neurons in a region of the lateral BNST that Swanson and colleagues (2001) have termed the anterolateral group ($BNST_{ALG}$; Dong et al. 2001), suggesting that the activation of this region may contribute to the expression of affective behaviors, such as those elicited by stressful stimuli. Consistent with this hypothesis, electrical stimulation of the BLA in vivo mimics the increased activation of $BNST_{ALG}$ neurons that is normally observed in response to stressful stimuli (Adamec 1989; Casada and Dafny 1992; Dalsass and Siegel 1987). Similarly, stimulation of the $BNST_{ALG}$ mimics many of the endocrine, cardiovascular, and respiratory responses that are elicited by stressful stimuli (Casada and Dafny 1991). Thus the $BNST_{ALG}$ may represent a critical node in the neural circuitry that functions to coordinate an appropriate affective response to stressful stimuli.

However, the $BNST_{ALG}$ is not a homogeneous structure and is composed of the anterolateral, subcommissural, oval, juxtacapsular, fusiform, and rhomboid nuclei (Dong et al. 2001). Moreover, although the majority (70–90%) of $BNST_{ALG}$ neurons can be classified as medium-sized spiny GABAergic neurons (McDonald 1983; Sun and Cassell 1993), at least three different subtypes have been identified based on either their somatic morphology (Larriva-Sahd 2006; McDonald 1983), their coexpression of peptide neurotransmitters, or their receptor pharmacology (Arluison et al. 1994; Gray and Magnuson 1992; Woodhams et al. 1983). Not surprisingly, therefore

Address for reprint requests and other correspondence: D. G. Rainnie, Emory University, Department of Psychiatry and Behavioral Science, Center for Behavioral Neuroscience, Yerkes Neuroscience Building, 954 Gatewood Road, Atlanta, GA 30329 (E-mail: drainni@emory.edu).

The costs of publication of this article were defrayed in part by the payment of page charges. The article must therefore be hereby marked "*advertisement*" in accordance with 18 U.S.C. Section 1734 solely to indicate this fact.

$BNST_{ALG}$ neurons also exhibit a heterogeneous response to local neurotransmitter release. Thus extracellular single-unit recording studies have shown that $BNST_{ALG}$ neurons can be either excited or/and inhibited by opiates (Casada and Dafny 1993; Dalsass and Siegel 1990), norepinephrine (NE) (Casada and Dafny 1993), acetylcholine (Casada and Dafny 1993), and oxytocin (Ingram et al. 1990). Thus even within discrete $BNST_{ALG}$ nuclei stressful stimuli may activate different categories of $BNST_{ALG}$ neurons.

More recently, we and others have shown that the response of individual $BNST_{ALG}$ neurons to neurotransmitters such as serotonin (5-HT) or NE depends on two interrelated factors: *1*) their postsynaptic receptor expression profile and *2*) their intrinsic membrane properties (Egli and Winder 2003; Levita et al. 2004; Rainnie 1999). Indeed, these initial current-clamp studies suggested that multiple, physiologically distinct cell types exist within subdivisions of the $BNST_{ALG}$ (Egli and Winder 2003; Rainnie 1999).

Here, we extend our initial current-clamp observations and describe three distinct physiological cell types within the $BNST_{ALG}$. Furthermore, using voltage-clamp analysis we have characterized the primary active currents that play a major role in shaping the physiological properties of these distinct cell types.

METHODS

Slice preparation

Before slice preparation, 24- to 48-day-old male Sprague–Dawley rats were housed four per cage and had unrestricted access to food and water. Care was taken to minimize the number of animals used; all procedures were done in accordance with policy guidelines set by the National Institutes of Health and were approved by the Emory University Institutional Animal Care and Use Committee. To obtain $BNST_{ALG}$ slices, rats were decapitated under isoflurane anesthesia (Abbott Laboratories, North Chicago, IL) and the brains rapidly removed and placed in ice-cold kynurenic acid–based artificial cerebrospinal fluid ($ACSF_{KA}$), which contained (in mM): NaCl (130), KCl (3.5), KH_2PO_4 (1.1), $MgCl_2$ (6.0), $CaCl_2$ (1.0), $NaHCO_3$ (30), glucose (10), and kynurenic acid (2). The glutamatergic antagonist kynurenic acid was included in the $ACSF_{KA}$ to suppress any unwanted effects of glutamate release that may occur during tissue slicing. Divalent cation levels were also adjusted to reduce the probability of neurotransmitter release. A block of tissue containing the BNST was then mounted on the chuck of a Leica VTS-1000 vibrating microtome (Leica Microsystems, Bannockburn, IL), and 350-μm coronal slices were cut. Slices were then hemisected and hand-trimmed to remove excess tissue lateral to the $BNST_{ALG}$. Slices were transferred to a holding chamber containing $ACSF_{KA}$ at room temperature and gassed with a 95% O_2-5% CO_2 mixture for 1 h before being placed in oxygenated control ACSF containing (in mM): NaCl (130), KCl (3.5), KH_2PO_4 (1.1), $MgCl_2$ (1.3), $CaCl_2$ (2.5), $NaHCO_3$ (30), and glucose (10). Experiments started a minimum of 0.5 h after the transfer of slices into the control ACSF.

Visual identification of $BNST_{ALG}$ neurons

Slices were placed in a Warner Series 20 recording chamber (Warner Instruments, Hamden, CT) mounted on the fixed stage of a Leica DM-LFS microscope (Leica Microsystems). Slices were fully submerged and continuously perfused at a rate of 1–2 ml/min with heated (32°C) and oxygenated ACSF. Neurons were visualized using infrared (IR) illumination and a ×40 water-immersion objective (Leica Microsystems). Images were captured using an IR-sensitive charge-coupled device (CCD) digital camera (Orca ER, Hamamatsu, Tokyo, Japan), coupled to a Meteor-II video frame grabber (Matrox Electronic Systems, Dorval, Canada), and displayed on a computer monitor using Simple PCI 6.11 software (Compix, Sewickley, PA).

Recording procedures

For whole cell patch-clamp recording, thin-walled borosilicate glass-patch electrodes (WPI, Sarasota, FL) were pulled on a Flaming/Brown micropipette puller (Model P-97, Sutter Instrument, Novato, CA). Patch electrodes had resistances ranging from 4 to 8 MΩ, when filled with a standard patch solution that contained (in mM): K-gluconate (138), KCl (2), $MgCl_2$ (3), phosphocreatine (5), K-ATP (2), NaGTP (0.2), and HEPES (10). The patch-recording solution was adjusted to a pH of 7.3 with KOH and had a final osmolarity of 280 mOsm. Whole cell patch-clamp recordings were obtained as previously described (Levita et al. 2004; Rainnie et al. 2004), using an Axopatch-1D amplifier (Molecular Devices, Sunnyvale, CA), a Digidata 1320A A-D interface, and pClamp 8.2 software (Molecular Devices). In cell-attached mode, patch electrode seal resistance was considered acceptable if it was $>$1.5 GΩ. For all experiments, whole cell patch-clamp configuration was initially established in current-clamp mode. Neurons were excluded from analysis if they showed a resting membrane potential (V_m) more positive than $-$55 mV and/or had an action potential that did not overshoot +5 mV. Subsequent data from current- and voltage-clamp recordings were sampled at rates determined by the speed of the measured response. In general, current-clamp data were filtered at 5 kHz and voltage-clamp data at 2 kHz. Access resistance for voltage-clamp protocols was monitored over the course of each experiment and was considered acceptable if it was $<$20 MΩ. Long-duration effects of drug application were recorded on a chart recorder (Kipp & Zonen, Bohemia, NY).

Drug application

Drugs were applied by gravity perfusion at the required concentration in the circulating ACSF. Drugs used included: cesium chloride (CsCl), 5 mM; nickel chloride ($NiCl_2$), 500 μM; 4-aminopyridine (4-AP), 1–10 mM; barium chloride ($BaCl_2$), 500 μM; bicuculline methiodide, 30 μM; verapamil hydrochloride, 100 μM; riluzole, 30 μM; tetrodotoxin (TTX), 1 μM, and tetraethylammonium chloride (TEA-Cl), 20 mM from Sigma–Aldrich (St. Louis, MO); and 3-[[(3,4-dichlorophenyl)methyl]amino]propyl] diethoxymethyl)phosphinic acid (CGP 52432), 1 μM; (*RS*)-3-(2-Carboxypiperazin-4-yl)-propyl-1-phosphonic acid [(*RS*)-CPP], 10 μM; 6,7-dinitroquinoxaline-2,3-dione (DNQX), 20 μM; and 4-(*N*-ethyl-*N*-phenylamino)-1,2-dimethyl-6-(methylamino) pyridinium chloride (ZD7228), 30–60 μM, purchased from Tocris (Ellisville, MO). All drugs were stored frozen as concentrated stock solutions in dH_2O except DNQX, which was made in 50% dimethyl sulfoxide and buffered to pH 7.3.

Statistics

Statistical analyses are described for each experiment in the following sections. All statistics were performed using GraphPad Prism version 4.02 (GraphPad Software, San Diego, CA).

Current-clamp characterization of the basic electrophysiological properties of $BNST_{ALG}$ neurons

A standardized series of current-clamp test protocols were conducted to determine the physiological characteristics of each neuron at a holding potential of $-$60 mV, unless otherwise stated. Thus the passive and active membrane properties of each neuron were primarily assessed by determining the voltage response to transient (750-ms), incremental current steps ranging from $-$75 to +25 pA. The membrane input resistance (R_m) was determined from the peak volt-

age response to a −5-pA current injection. The properties of single action potentials were determined using short-duration (10-ms), high-amplitude (15- to 115-pA), incremental current injections. Based on the readout of these protocols, neurons were assigned to one of three groups: Type I, Type II, or Type III (see Fig. 2). Statistical comparisons between these groups were made using one-way ANOVA for each of the following variables: V_m; R_m; time constant for membrane charging (τ); action-potential threshold, amplitude, rise- and decay times, and half-width. A post hoc Tukey's multiple comparison test (MCT) was conducted to determine individual group differences.

Voltage-clamp characterization of the intrinsic membrane currents of BNST$_{ALG}$ neurons

The characteristic voltage response of Type I–Type III BNST$_{ALG}$ neurons suggested that several cell type–specific intrinsic membrane currents may be expressed by these neurons. The following voltage-clamp experiments were conducted to more fully characterize these currents.

HYPERPOLARIZATION-ACTIVATED NONSELECTIVE CATION CURRENT (I_H). Type I and Type II neurons showed a time-dependent depolarizing sag in the voltage response to hyperpolarizing current injection (see Fig. 2), which was reminiscent of that mediated by activation of the hyperpolarization-activated nonselective cation current (I_h) in other regions of the CNS (for review, see Roberts and Seigelbaum 2003). To isolate and characterize the properties of I_h-like currents, the ACSF was supplemented with 1 μM tetrodotoxin (TTX) and 500 μM $NiCl_2$ to block sodium- and low-threshold T-type calcium currents, respectively. The voltage dependency of I_h activation was determined using a dual-step protocol (McCormick and Pape 1990). Here, steady-state I_h activation was determined by applying a conditioning step command to potentials ranging from −100 to −45 mV for 1.5 s. The membrane potential was then stepped to −85 mV, as illustrated in Fig. 4, and the peak of the resulting "tail" current measured, normalized to a percentage of the maximum tail current response, and plotted as a function of the voltage achieved during the conditioning step. The normalized steady-state activation curve was then fit with a Boltzmann equation of the form

$$I = 1/\{1 + \exp[(V - V_{50})/k]\} \quad (1)$$

where I is the normalized current, V_{50} is the half-maximal membrane potential, and k describes the slope. The inclusion of either CsCl (5 mM) or ZD7228 (30 μM) in the ACSF blocked the tail current. The significance of drug effect was determined using an F-test to compare the control activation curves with those obtained in the presence of the I_h channel blockers.

To compare I_h activation kinetics across cell types, we determined the time constant of I_h activation (τ_h) in response to a standardized transient (600-ms) voltage step from −60 to −100 mV, where τ_h was determined as the time taken to reach 1/e of the steady-state current calculated using a single-exponential best-fit subroutine of Clampfit software (Molecular Devices). A frequency histogram of the τ_h value for each neuron was constructed and the distribution was best fit by the sum of two Gaussian curves of the form

$$Y = \text{amplitude} \times \exp\{-0.5[(X - \text{mean})/\text{SD}]^2\} \quad (2)$$

where amplitude is the peak response, exp is the base of the natural logarithm, mean is the average time constant, and standard deviation is the SD of the distribution.

LOW-THRESHOLD CALCIUM CURRENT (I_T). To isolate and characterize the properties of I_T, the stock ACSF was adjusted to the following composition (in mM): NaCl (120), KCl (3.5), HEPES (10), TEA-Cl (20), $MgCl_2$ (1.3), $CaCl_2$ (2.5), 4-AP (1.0), CsCl (5.0), TTX (0.001), $NaHCO_3$ (30), and glucose (10). TEA-Cl and 4-AP were included to suppress depolarization-activated outward potassium currents (see following text) and CsCl was included to suppress I_h. A dual-step protocol was used to examine the current–voltage relationship of I_T activation. Here, the membrane potential was stepped to −90 mV for 500 ms and then stepped to command potentials ranging from −60 to −40 in increments of 5 mV for 500 ms. Peak inward currents were normalized to the maximum evoked current [$I_T/I_{T(max)}$] and plotted as a function of the command voltage. Steady-state leak currents were subtracted from the raw data using the leak-subtraction subroutine of Clampfit software. Data were then fit with a Boltzmann equation (*Eq. 1*). Leak current was assumed to be linear and was corrected using the following equation

$$\text{Corrected current} = (\text{Original current} - \text{Stimulus waveform})/(0.001R_m) \quad (3)$$

The time constant of I_T decay (τ_T; deactivation) was determined by fitting a single exponential to the decay phase of the peak I_T current using the best-fit subroutines of Clampfit software. τ_T was determined as the time taken to reach 1/e of the peak current.

I_T channels inactivate close to the resting membrane potential of many neurons and require a period of membrane hyperpolarization to deinactivate before activation (see Perez-Reyes 2003). To examine the deinactivation kinetics of I_T, the membrane potential was stepped from −60 to −100 mV for 500 ms in 10-mV increments and then stepped to a command potential of −50 mV for 500 ms. Peak I_T amplitude was normalized to $I_{T(max)}$ and plotted as a function of the conditioning voltage. Leak currents were subtracted from the raw data (see above), data were fit with a Boltzmann equation (*Eq. 1*), and the half-maximal activation voltage was determined.

To examine the temporal kinetics of I_T deinactivation ($\tau_{deinact}$) and inactivation (τ_{inact}) we used two additional dual-step protocols. Here, $\tau_{deinact}$ was determined by varying the duration of the conditioning prepulse from 100 ms to 1 s, in 100-ms increments, and plotting the peak I_T amplitude evoked by a command step to −50 mV as a function of the prepulse duration. Leak-corrected currents were normalized to the maximum current and data were fit with a single-exponential association equation

$$I = I_{max}(1 - e^{-Kt}) \quad (4)$$

where I is the normalized current, t is time, I_{max} is the maximum current attained (near 1), and K is the rate constant. To determine τ_{inact}, the time between a fixed-amplitude (−100 mV) conditioning prepulse and the command step (−50 mV) was increased from 15 to 555 ms in 60-ms increments. Peak currents were corrected for leak, normalized to the maximum evoked current, and plotted as a function of the interval between the conditioning and the activation steps. Data were fitted with a single-exponential decay equation

$$I = I_{max}e^{-Kt} + I_{sst} \quad (5)$$

where I is the normalized current, t is time, I_{max} is the peak current, I_{sst} is the steady-state current, and K is the rate constant.

TRANSIENT OUTWARD POTASSIUM CONDUCTANCE (I_A). Our initial I_T studies suggested that this current was tightly regulated by a transient outward current, which had activation kinetics and a voltage dependency similar to those reported for the transient outward potassium current I_A. To isolate and further characterize this current, the ACSF was adjusted to the following composition (in mM): NaCl (110), KCl (3.5), TEA-Cl (20), KH_2PO_4 (1.1), $MgCl_2$ (3.3), $CaCl_2$ (0.5), $CdCl_2$ (0.15), $NiCl_2$ (0.5), TTX (0.001), verapamil (0.1), $NaHCO_3$ (30), ZD7228 (0.06), and glucose (10). Here, TEA-Cl was included to block both outwardly rectifying and some calcium-dependent potassium currents. A cocktail of $CdCl_2$, verapamil, and $NiCl_2$ was included to maximally block calcium currents. Unless otherwise noted, all I_A voltage-clamp protocols were conducted from a holding potential of −40 mV.

To examine the voltage dependency of I_A, activation and deinactivation dual-step protocols similar to those outlined earlier for I_T

were used. With respect to I_T analyses, I_A current responses were leak corrected, normalized to the maximum current response, and plotted as a function of the command voltage. Data were fit with a Boltzmann equation (*Eq. 1*). The time constant of I_A decay (τ_A) was determined by fitting an exponential curve to the decay phase of the I_A current; τ_A was determined as the time taken to reach 1/*e* of the steady-state current. I_A decay was best fit using the dual-exponential subroutine of Clampfit software. To determine whether the rate of I_A decay was voltage dependent, τ_A was plotted as a function of command voltage and a regression coefficient calculated for each time constant.

The deinactivation time constant ($\tau_{deinact}$) for I_A was determined using a dual-step protocol similar to that used for I_T. Here the duration of the conditioning prepulse was increased from 50 to 700 ms in 50-ms increments, followed by a 500-ms command step to −25 mV. To improve the temporal resolution of this protocol (see *inset* of Fig. 7) shorter (10-ms) increments were used such that the duration of the conditioning prepulse varied from 10 to 110 ms. Similar to I_T, the inactivation time constant (τ_{inact}) was determined using a protocol in which the interval between the prepulse and the command step increased from 0 to 900 ms in increments of 100 ms. Analyses were conducted on the peak outward current elicited at the beginning of each command step. Current responses were corrected for leak, normalized to the maximum current response, and plotted as a function of the duration between the first and second steps. Data were fitted with a one-phase exponential-decay equation (*Eq. 5*).

INWARDLY RECTIFYING POTASSIUM CURRENT [$I_{K(IR)}$]. A characteristic of Type III neurons was that they exhibit a time-independent depolarizing rectification in the voltage response to hyperpolarizing current injection of increasing amplitude (see Fig. 2). This rapid anomalous rectification was reminiscent of that produced after activation of members of the family of inwardly rectifying potassium channels (K_{IR}; see Nichols and Lopatin 1997). The current underlying the anomalous rectification was examined in voltage-clamp mode using a standard hyperpolarization protocol in which the voltage command was stepped from −60 to −100 mV for 600 ms in 10-mV increments.

PERSISTENT SODIUM CURRENT (I_{NaP}). In some $BNST_{ALG}$ neurons, the kinetics of decay for the voltage response to transient (10-ms) depolarizing current injection far outlasted that predicted by the τ_m of these neurons. The long duration and voltage-sensitivity of the potential decay were similar to those previously reported after activation of the noninactivating voltage-dependent sodium current I_{NaP} (also called the persistent sodium current). To determine whether $BNST_{ALG}$ neurons express I_{NaP}, the ACSF was adjusted to the following composition (in mM): NaCl (34), KCl (5), $MgCl_2$ (3), $CaCl_2$ (2), BaCl (2), TEA-Cl (80), 4-AP (4), CsCl (3), CdCl (0.2), glucose (10), and $NaHCO_3$ (30). In addition, the patch pipette solution was modified to one that contained (in mM): $CsMeSO_4$ (120), TEA (3), $MgCl_2$ (1), HEPES (10), phosphocreatinine (10), K-ATP (2), and Na-GTP (0.2). Using these two solutions in combination allowed us to block most of the intrinsic currents outlined earlier, to isolate I_{NaP}. The sodium concentration was reduced to 34 mM and replaced by TEA-Cl to prevent action potential generation. The voltage dependency of I_{NaP} was examined using a voltage-ramp protocol (Urbani and Belluzzi 2000) in which the command voltage was ramped from −100 to +10 mV at a rate of 10 mV/s. I_{NaP} was observed as a transient inward current activating at approximately −46 mV.

RESULTS

Cell types of the $BNST_{ALG}$

In the course of our ongoing studies of the pharmacological (Levita et al. 2004) and physiological (Rainnie 1999) properties of $BNST_{ALG}$ neurons, we have recorded from over 276 neurons. For these studies all recordings were made from neurons located in the lateral $BNST_{ALG}$ dorsal to the anterior commissure, which consists of the anterolateral area proper, the oval nucleus, rhomboid nucleus, and the juxtacapsular nucleus of the $BNST_{ALG}$ as defined by Dong and Swanson (2004) (see Fig. 1). For each $BNST_{ALG}$ neuron included in these studies, we routinely conducted a series of standardized current-clamp protocols (see METHODS) to determine their characteristic voltage response to transient depolarizing and hyperpolarizing current injection. Based on several characteristic voltage trajectories, $BNST_{ALG}$ neurons could be categorized into three distinct cell types (Type I–Type III). Thus neurons were categorized according to the presence or absence of *1*) a time-dependent depolarizing sag in the voltage response to hyperpolarizing current injection, which exhibited a rebound depolarization on termination of the current pulse (Fig. 2*B*, Type I and Type II); *2*) an enhanced rebound depolarization on termination of the hyperpolarizing current steps, which exceeded that previously described, and which was often of sufficient magnitude to trigger action potentials (Fig. 2*B*, Type II); *3*) a time-independent depolarizing rectification of the voltage response to hyperpolarizing current injection, which did not exhibit any rebound depolarization on termination of the current injection (Fig. 2*B*, Type III); and *4*) their action potential firing pattern triggered in response to transient depolarizing current injection (Fig. 2*A*).

TYPE I NEURONS. Type I neurons accounted for 29% of all recorded $BNST_{ALG}$ neurons, had a resting membrane potential (V_m) of −60.0 ± 0.6 mV, and a mean input resistance (R_m) of 452.6 ± 30.0 MΩ. As shown in Table 1, a significant difference was observed in both the R_m [$F(2,226) = 16.02$, $P < 0.05$] and V_m [$F(2,275) = 3.6$, $P < 0.05$] across the three cell

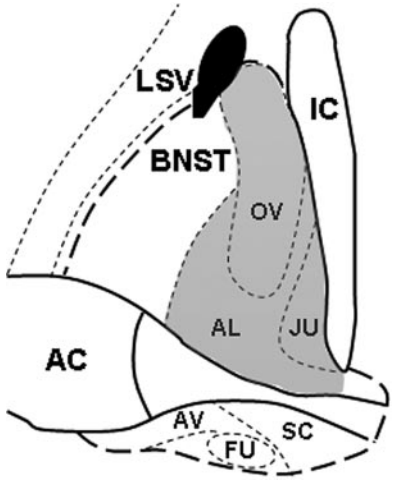

FIG. 1. Anterolateral group of the bed nucleus of the stria terminalis ($BNST_{ALG}$), as defined by Dong et al. (2001), is outlined by the thicker hatched line. In the present studies, neurons were recorded from the lateral $BNST_{ALG}$ regions outlined in gray. Neurons were recorded from regions dorsal to the anterior commissure, including the anterolateral area proper, the oval nucleus, rhomboid nucleus, and the juxtacapsular nucleus. AC, anterior commissure; AV, anteroventral area; AL, anterolateral area; BNST, bed nucleus of the stria terminalis; FU, fusiform nucleus; IC, internal capsule; JU, juxtacapsular nucleus; LSV, ventral lateral septal nucleus; OV, oval nucleus; SC, subcommissural zone.

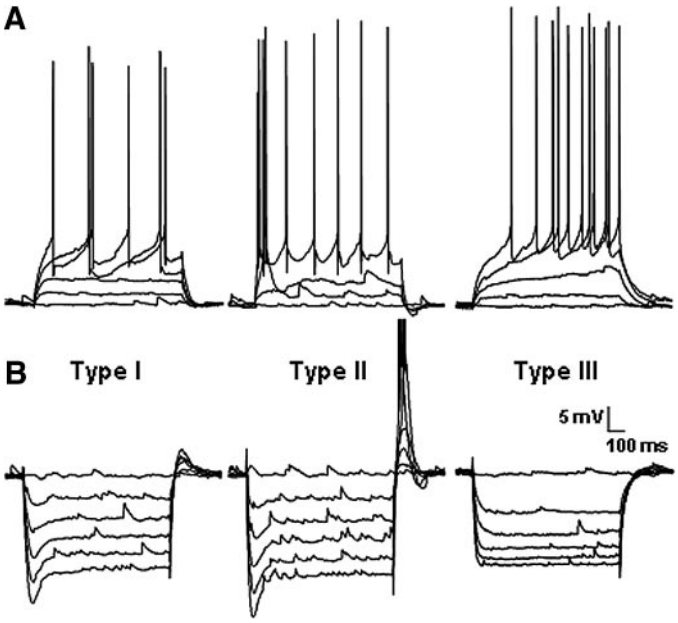

FIG. 2. Three electrophysiologically distinct cell types (I–III) are observed in the $BNST_{ALG}$ differ in their response to depolarizing and hyperpolarizing current injection. *A*: Type II neurons respond to depolarizing current injection with an initial burst of spikes followed by a more regular firing pattern, whereas Type I and Type III fired with a regular firing pattern. *B*: Type I and Type II neurons exhibited a depolarizing sag in response to hyperpolarizing current injection that was accompanied by a rebound depolarization on the offset of current injection. In Type II neurons this rebound event was often accompanied by spikes. Type III neurons did not exhibit the depolarizing sag, but instead exhibited a fast anomalous rectification at more hyperpolarized potentials.

types. In contrast, no significant difference was seen for the τ [$F(2,59) = 0.44$, $P > 0.05$]. For both V_m and R_m, Tukey's MCT revealed that Type I neurons differed significantly from Type III neurons, but not from Type II neurons.

In response to transient (750-ms) hyperpolarizing current injection, Type I neurons exhibited a characteristic depolarizing sag (rectification) in their voltage response that was both time dependent and voltage dependent, such that the amplitude and rate of onset of the rectification increased with increasing membrane hyperpolarization (see Fig. 2*B*, Type I). The input resistance measured at the peak of the hyperpolarizing voltage response was always greater than that determined once the rectification had reached a steady-state level, suggesting that the sag was mediated by a voltage-dependent increase in membrane conductance. Type I neurons also exhibited a transient depolarizing rebound potential on termination of the hyperpolarizing current injection, the amplitude and rate of onset of which also increased with increasing levels of initial membrane hyperpolarization. Significantly, the amplitude and rate of onset of the rebound depolarization mirrored the level of the depolarizing rectification observed in the voltage response during hyperpolarizing current injection, suggesting that they were mechanistically connected. Similar properties have been previously reported in neurons from multiple brain regions after activation of the hyperpolarization-activated nonselective cation current I_h (for review, see Roberts and Seigelbaum 2003). By comparison, the voltage response to transient depolarizing current injection was relatively linear until the threshold for action potential generation was reached.

In response to suprathreshold depolarizing current injection, Type I neurons exhibited a regular firing pattern, such that the first interspike interval (ISI, 110.8 ± 8.7 ms) did not significantly differ ($t = 0.01$, $P < 0.05$, $n = 40$) from the last ISI (154.5 ± 11.9 ms). On average, single action potentials had a threshold for activation of −43.2 ± 0.5 mV, an amplitude of 75.7 ± 3.9 mV, a 10–90% rise time of 0.44 ± 0.02 ms, a 90–10% decay time of 0.88 ± 0.05 ms, and a half-width of 0.95 ± 0.04 ms. These properties are summarized in Table 1 and compared with those of Type II and Type III neurons. As illustrated in Table 1, spike properties did not significantly differ between cell types.

TYPE II NEURONS. Type II neurons were the most abundant of $BNST_{ALG}$ neurons, accounting for 55% of all recorded cells. These neurons had a V_m of −58.0 ± 0.5 mV and an R_m of 377.4 ± 15.7 MΩ. Type II neurons also exhibited a depolarizing sag in response to hyperpolarizing current injection that was similar to that described for Type I neurons. However, in contrast to Type I neurons, the amplitude and rate of onset of the rebound depolarization observed at the termination of the hyperpolarizing current injection were always much larger than the degree of depolarizing rectification observed. Significantly, the amplitude of the rebound depolarization often surpassed action potential threshold and triggered a rebound burst of action potentials (see Fig. 2*B*, Type II), suggesting that Type II neurons express additional active currents that could be modulated by prior membrane hyperpolarization.

Unlike Type I neurons, the response of Type II neurons to transient depolarizing current injection was nonlinear. Thus, in Type II neurons subthreshold depolarizing current injection

TABLE 1. *Properties of Type I, Type II, and Type III neurons*

	Type I	Type II	Type III
Percentage, %	29	55	16
V_m, mV	−60.6 ± 0.59	−58.4 ± 0.49	−64.8 ± 1.07*
R_m, MΩ	452.6 ± 30†	377.4 ± 15.6	357.8 ± 38.1
τ, ms	32.7 ± 3.1	31.44 ± 2.7	29.22 ± 2.0
Spike			
Threshold for activation, mV	−43.2 ± 0.5	−44.2 ± 0.6	−42.75 ± 0.8
Amplitude, mV	75.7 ± 3.9	82.0 ± 3.7	69.3 ± 4.9
Rise time, ms	0.44 ± 0.02	0.49 ± 0.03	0.42 ± 0.02
Decay time, ms	0.88 ± 0.05	1.04 ± 0.09	1.0 ± 0.12
Half-width, ms	0.95 ± 0.04	1.1 ± 0.09	0.96 ± 0.06

Values are means ± SE. *Statistically significant from Type I and Type II. †Statistically significant from Type II, but not Type III.

evoked a depolarizing "hump" that peaked within 150 ms of the onset of current injection and that became more pronounced at membrane potentials at, or near, threshold for action potential firing. Expression of this transient depolarizing potential caused Type II neurons to exhibit a burst-firing pattern, which was characterized by a rapid succession of action potentials followed by a delay before the onset of the next spike or succession of spikes (Fig. 2*A*, Type II). Winder and coworkers (2003) reported a similar transient depolarizing potential in ventral BNST neurons that was blocked by $NiCl_2$ (200 μM), a concentration that preferentially blocks the low-threshold calcium current I_T (Egli and Winder 2003), suggesting that Type II neurons of the $BNST_{ALG}$ might also express the I_T current.

After the initial burst of action potentials, Type II neurons either fire in a regular pattern (Fig. 2*A*, Type II), fire in bursts, or stop firing altogether (accommodate). The variability of this second response is likely explained by the differential expression of outward rectifying currents and calcium-dependent potassium currents, and/or differences in the properties of the calcium currents that generate the initial burst. These differences suggest that even within Type II neurons there is heterogeneity in their physiological responses. Unlike the net action potential firing pattern, the properties of single spikes evoked in Type II neurons did not differ significantly from those described for Type I or Type III neurons (see Table 1).

TYPE III NEURONS. Type III neurons made up 16% of recorded $BNST_{ALG}$ neurons, had a V_m of -64 ± 1.1 mV, and an R_m of 357.8 ± 38.1 MΩ. Unlike Type I and Type II neurons, Type III neurons did not show a prominent time-dependent depolarizing sag in response to hyperpolarizing current injection. Instead, Type III neurons exhibited a fast time-independent rectification that became more pronounced with increased amplitude of current injection (Fig. 2*B*, Type III). Unlike the time-dependent rectification observed in Type I and Type II neurons, no rebound depolarization was observed in Type III neurons on the termination of the hyperpolarizing current injection. These properties are similar to those previously reported in other brain regions after activation of an inwardly rectifying potassium current K_{IR} (De Jeu et al. 2002; Nisenbaum and Wilson 1995), which suggested that Type III neurons may preferentially express this current.

In response to depolarizing current injection, Type III neurons fired with a regular firing pattern; like Type I neurons the first ISI (65.8 ± 8.2 ms) did not significantly differ ($t = 0.07$, $P < 0.05$, $n = 40$) from the last ISI (82.1 ± 9.3 ms). However, Type III neurons showed a significantly longer latency to first spike onset [$F(2,59) = 29.21$, $P < 0.05$] than did Type I and Type II neurons (data not shown).

Intrinsic membrane currents of $BNST_{ALG}$ neurons

Having categorized $BNST_{ALG}$ neurons into three physiologically distinct subtypes based on our current-clamp data, we next recorded neurons in voltage-clamp mode to isolate and characterize some of the intrinsic membrane currents that act to shape the voltage response of these neurons. We present below, the biophysical properties of the five most prominent membrane currents expressed by one or more subtypes of $BNST_{ALG}$ neuron. It should be noted that these data are not presented in any particular order of importance.

EXPRESSION OF THE NONSELECTIVE CATION CURRENT (I_H). Approximately 84% of BNST neurons display a time-dependent rectification of the voltage response to hyperpolarizing current injection (Fig. 3*B*; see also Egli and Winder 2003; Rainnie 1999). Because the rectification was similar in many ways to that previously reported as being mediated by activation of I_h channels, we first examined the response of $BNST_{ALG}$ neurons to addition of the nonspecific I_h channel blocker CsCl (5 mM, $n = 13$) to the ACSF. In current clamp, application of CsCl completely blocked the depolarizing sag (not

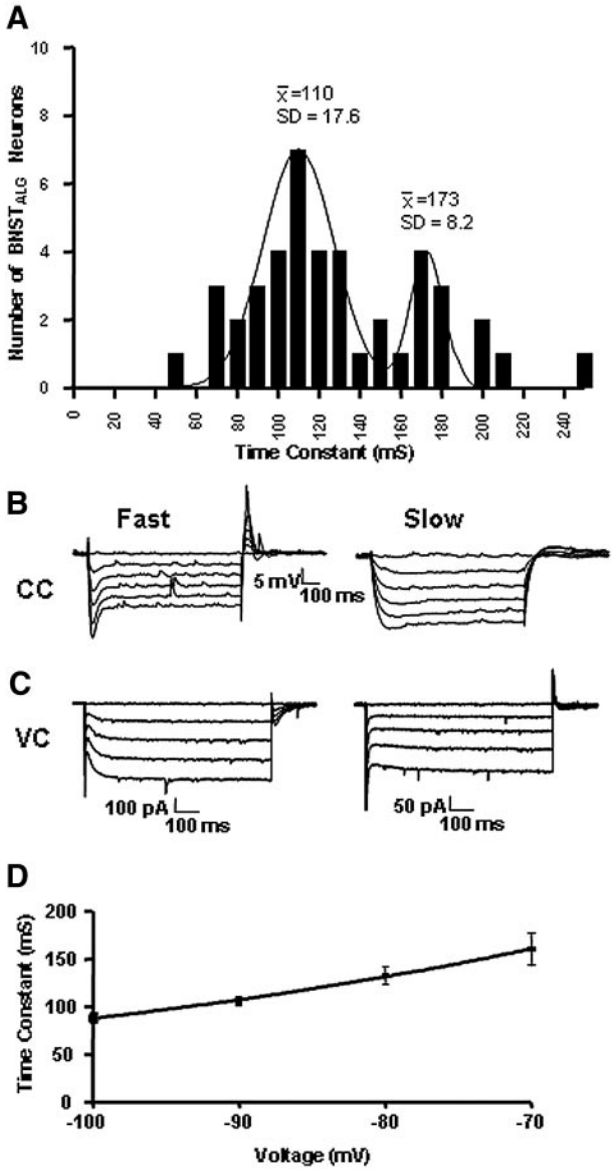

FIG. 3. Depolarizing sag in the $BNST_{ALG}$ activated with different time constants. *A*: frequency distribution of time constant values for the depolarizing sag across all $BNST_{ALG}$ neurons. *B*: example in current-clamp mode (CC) of fast and slowly activating depolarizing sags. *C*: examples in voltage-clamp mode (VC) of fast and slowly activating inward currents mediating the fast and slowly activating depolarizing sags. *D*: time constant of the inward current mediating the depolarizing sag decreased as neurons were stepped to more hyperpolarized levels from -60 mV.

shown), increased R_m by 161.6 ± 12.2%, and caused a −4.2 ± 1.8-mV hyperpolarizing shift in resting membrane potential, suggesting that the majority of $BNST_{ALG}$ neurons actively express I_h channels and that tonic activation of I_h channels plays a significant role in regulating both the V_m and the R_m of these neurons.

In voltage clamp, the depolarizing sag was associated with the activation of a time- and voltage-dependent inward current. The time constant for current activation (τ_h), measured as the time taken for the current to reach 1/*e* of the maximal steady-state level in response to a voltage step from −60 to −80 mV, ranged from 47.7 to 254.1 ms. The population distribution of τ_h is illustrated in Fig. 3*A*. As can be seen, τ_h exhibited a bimodal distribution that was best fit with a biphasic Gaussian equation rather than a single Gaussian [$F(1,22) = 9.7$, $P < 0.05$]. These data suggested that those $BNST_{ALG}$ neurons expressing I_h could be further differentiated into "fast" and "slow" τ_h neurons based on their I_h kinetics. The mean τ_h value for the "fast" I_h subgroup was 110 ± 2.1 ms and for the "slow" I_h subgroup was 173 ± 2.5 ms.

In agreement with observations of I_h kinetics elsewhere in the brain (Morris et al. 2004; Roberts and Greene 2005), the rate of activation of the I_h-like current increased as the command potential became more negative (Fig. 3*D*). Thus transient hyperpolarizing step commands to −70 mV from a holding potential of −60 mV evoked an I_h-like current with a time constant of activation $\tau_h = 160.6 \pm 17.8$ ms, whereas steps commands to −100 mV evoked an I_h-like current with significantly faster kinetics, $\tau_h = 88.4 \pm 4.4$ ms ($t = 3.98$, $P < 0.05$, $n = 78$).

To examine the kinetics of the I_h-like current in greater detail, we used a dual-step voltage-clamp protocol and a modified ASCF that blocked concurrent activation of unwanted currents (see METHODS). A typical example of an intrinsic I_h-like "tail" current in a $BNST_{ALG}$ neuron is illustrated in Fig. 4*B* (*inset*). As reported previously (Morris et al. 2004), the amplitude of the I_h-like tail current was dependent on the voltage attained during the conditioning prepulse and showed a maximal amplitude of −96.8 ± 9.7 pA with prepulse steps to −120 mV. Fitting the data with a Boltzmann equation revealed a half-maximal activation voltage $V_{1/2} = -80.13 \pm 0.5$mV ($n = 6$) and a slope factor of −11.7 ± 0.5 mV (Fig. 4*C*). Inclusion of CsCl (5 mM) in the modified ACSF fully blocked the I_h-like "tail" current (Fig. 4*B*, *inset*). Moreover, application of the specific I_h channel blocker ZD7228 (30 μM) caused a time-dependent attenuation of the "tail" current [$F(3,114) = 49.8$, $P < 0.05$; data not shown], further suggesting that this was indeed mediated by activation of I_h channels.

EXPRESSION OF THE T-TYPE CALCIUM CURRENT (I_T). Type II neurons were identified primarily by their tendency to burst fire in response to depolarizing current injection and at the offset of hyperpolarizing current injection (Fig. 2*B*, Type II). Consistent with earlier reports (Egli and Winder 2003), addition of $NiCl_2$ (500 μM, $n = 9$) to the extracellular ACSF fully blocked burst firing in Type II neurons (data not shown), suggesting that

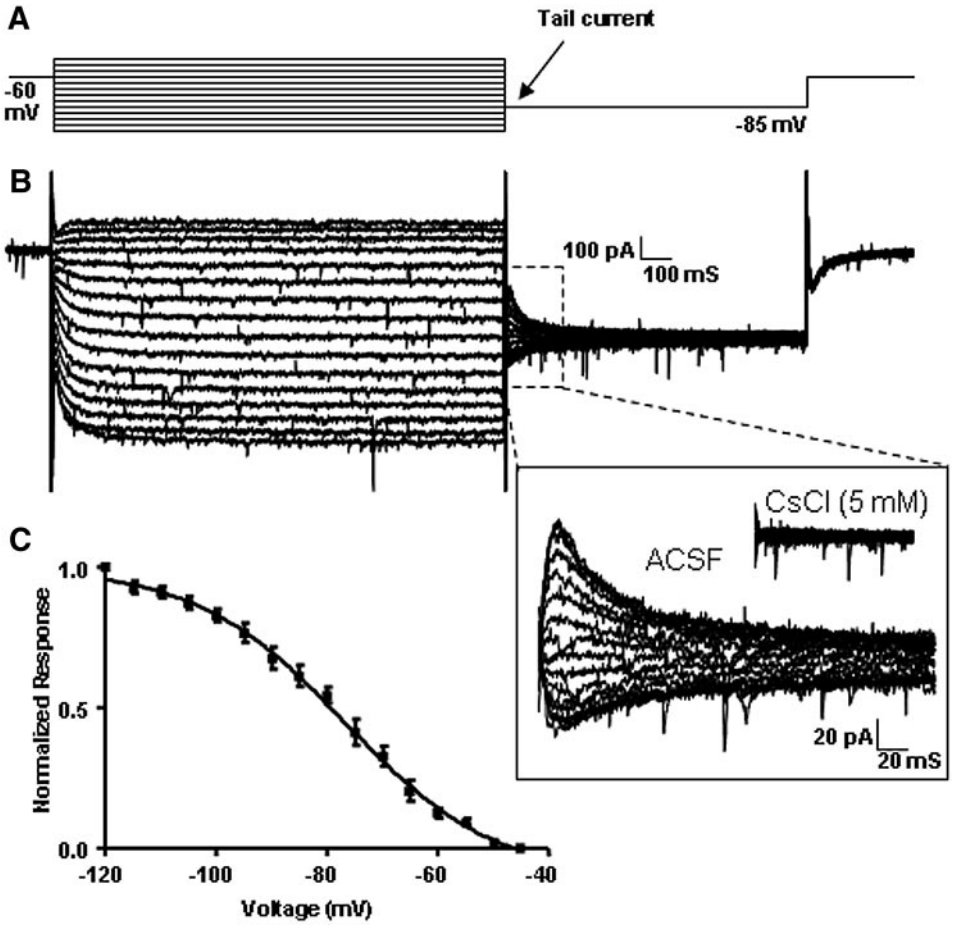

FIG. 4. A hyperpolarization-activated cation current (I_h)–like inward current mediated the depolarizing sag in $BNST_{ALG}$ neurons. *A*: dual-step protocol used to determine current activation properties. Neurons were stepped from −100 to −45 mV and then stepped to −85 mV. Tail current analyses were conducted on the current produced at the beginning of the second step. *B*: example of the current response induced by the protocol described in *A*. Tail current induced at the beginning of the second step is magnified in the box on the *bottom right*. This tail current was completely blocked in 5 mM of the I_h channel blocker CsCl (*inset*). *C*: activation properties of the I_h-mediated inward current. Normalized tail current is plotted as a function of the voltage attained in the conditioning step, and exhibited a half-maximal activation voltage ($V_{1/2}$) of −80.13 ± 0.5 mV.

burst firing in these neurons may be mediated by activation of the low-threshold calcium current I_T.

To further investigate whether $BNST_{ALG}$ neurons express an I_T-like current we used a dual-step voltage-clamp protocol (Fig. 5*A*) in association with a modified ACSF to isolate intrinsic calcium currents (see METHODS). Typically, I_T calcium channels require a period of membrane hyperpolarization to deinactivate before they can be activated by subsequent membrane depolarization (for review, see Perez-Reyes 2003). Consequently, we investigated the activation properties of the I_T-like current using a transient (500 ms) hyperpolarizing prepulse to −90 mV, to increase the probability of I_T channel deinactivation, followed by a series of depolarizing step commands of increasing amplitude. A typical example of the series of transient, inward, I_T-like currents generated in response to the dual-step protocol is illustrated in Fig. 5*A*. As expected, the dual-step protocol evoked a series of transient inward currents that increased in amplitude with increasing depolarizing step commands and that reached a peak amplitude of −102.0 ± 25.1 pA with step commands to −45 mV ($n = 6$). Moreover, the rate of rise of the I_T-like current increased significantly with increasing depolarizing step commands ($t = 3.81$, $P < 0.05$, $n = 13$), such that the time to peak with steps to −50 mV was 34.1 ± 3.2 ms, compared with 21.3 ± 2.3 ms for steps to −35 mV. In contrast, the rate of decay of the I_T-like current was relatively constant with a time constant for decay, $\tau_T = 19.9$ ms, irrespective of the voltage achieved ($n = 4$). We next examined the voltage dependency of I_T activation. As illustrated in Fig. 5*A*, the I_T-like current activated from membrane potentials close to −60 mV had a half-maximal activation potential ($V_{1/2}$) of −50.0 ± 0.5 mV and a slope factor of 2.4 ± 0.8 mV ($n = 5$).

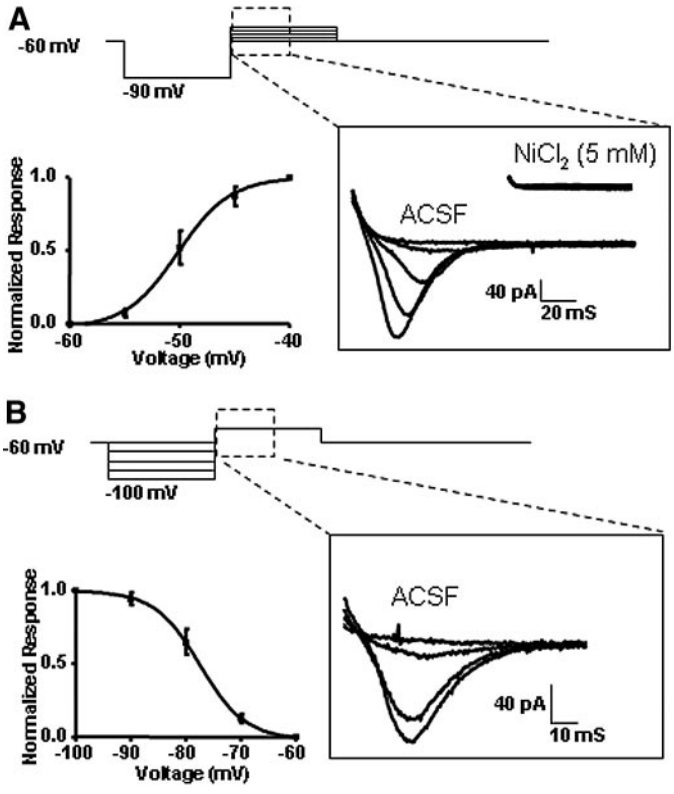

FIG. 5. $BNST_{ALG}$ neurons exhibit an inward current with properties of the low-threshold calcium current I_T. *A*, *top trace*: activation curve used to elicit the low-threshold calcium current I_T. An example of the inward currents evoked at the beginning of the second step is shown in the box on the *bottom right*. Current was completely blocked by the I_T channel blocker $NiCl_2$ (5 mM, *inset*). Activation curve revealed a $V_{1/2}$ of −50.00 ± 0.46 mV. *B*, *top trace*: dual-step protocol used to determine the deinactivation curve for the low-threshold calcium current I_T. An example of the inward currents evoked at the beginning of the second step is shown in the box on the *bottom right*. Deinactivation curve of the normalized response plotted as a function of the conditioning voltage revealed a $V_{1/2}$ of −77.65 ± 0.67 mV.

To examine the voltage dependency of deinactivation we used a similar dual-step protocol, except here the amplitude of the hyperpolarizing prepulse was varied and the amplitude of the subsequent depolarizing step command remained constant. As before, the peak inward current evoked during the depolarizing step command was normalized to the maximal evoked inward current and plotted as a function of membrane potential (see Fig. 5*B*). Here, the amplitude of the normalized peak inward current increased as a function of the amplitude of the hyperpolarizing step command, showing a half-maximal voltage for deinactivation ($V_{1/2}$) of −77.6 ± 0.6 mV and a slope factor of −4.0 ± 0.6 mV ($n = 7$) when fit with a Boltzmann equation.

Significantly, the I_T-like inward current was completely blocked after addition of 500 μM $NiCl_2$ to the ACSF (Fig. 5*A*, *inset*; $n = 5$) and significantly attenuated by addition of the I_T channel blocker mibefradil [10 μM; $F(1,85) = 44.7$, $P < 0.05$; data not shown], suggesting that the transient inward current observed in $BNST_{ALG}$ neurons was indeed mediated by the opening of low-threshold T-type calcium channels.

We next examined the temporal kinetics of deinactivation and inactivation of the I_T current in $BNST_{ALG}$ neurons. We reasoned that the time constant of deinactivation ($\tau_{deinact}$) would give a first approximation of the time required for an inhibitory postsynaptic event to significantly increase the probability of I_T channel opening in $BNST_{ALG}$ neurons on subsequent depolarization. Here, $\tau_{deinact}$ was determined by varying the duration of a hyperpolarizing prepulse, which preceded a depolarizing step command of fixed amplitude (Fig. 6*A*). The normalized I_T current was then plotted as a function of the duration of the preceding hyperpolarizing prepulse. As expected, the I_T amplitude increased with increasing prepulse duration and showed an *e*-fold increase ($\tau_{deinact}$) with a prepulse duration of 208.0 ms ($n = 5$; see Fig. 6*A*). Thus in $BNST_{ALG}$ neurons inhibitory synaptic events of approximately 200 ms duration could significantly facilitate any subsequent excitatory synaptic input by deinactivating I_T channels.

However, excitatory synaptic input onto BNST neurons fluctuates stochastically and would not always occur immediately after an inhibitory synaptic input. Consequently, we next examined the temporal domain in which an inhibitory synaptic input may continue to influence (facilitate) subsequent excitatory inputs (τ_{inact}). Here, the interval between the offset of the hyperpolarizing prepulse and the onset of the depolarization step command was incrementally increased (see Fig. 6*B*). The normalized I_T current was then plotted as a function of the interval duration. As illustrated, I_T amplitude decreased with increasing duration of the interpulse interval and showed an *e*-fold decrease in amplitude, τ_{inact}, of 56.1 ms ($n = 5$; see Fig. 6*B*). Thus the temporal kinetics of I_T channels in Type II neurons may function as a "memory" of the preceding inhibitory event, thereby defining a time window during which any subsequent excitatory synaptic input may be facilitated.

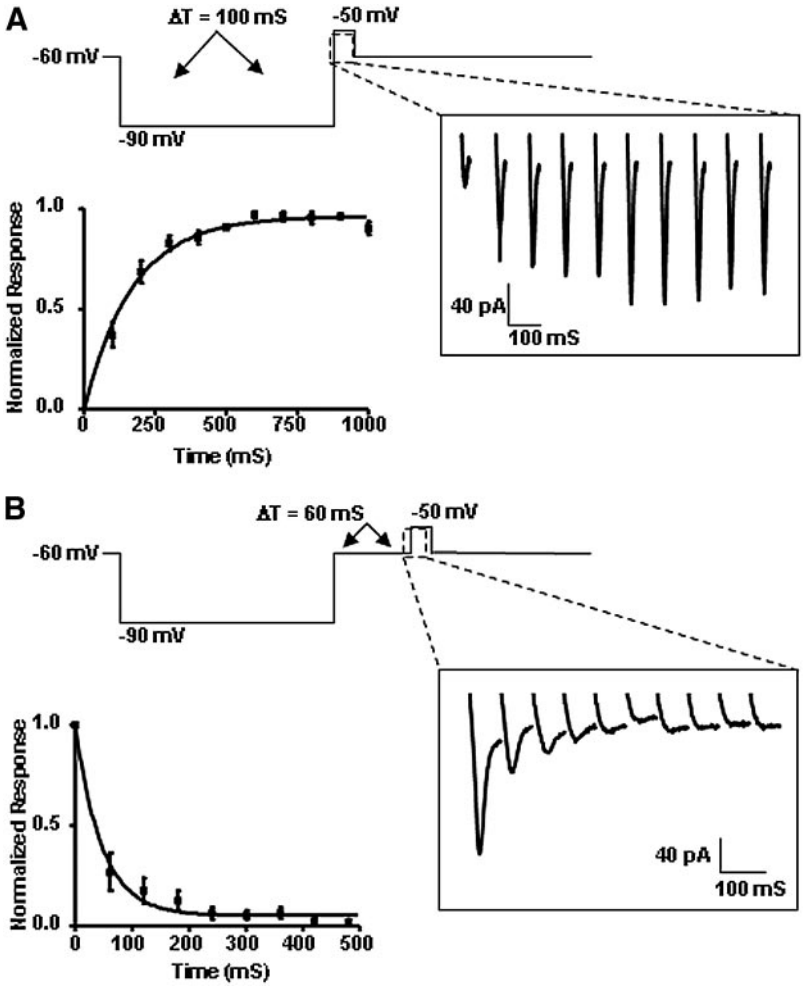

FIG. 6. Deinactivation and inactivation kinetics of the low-threshold calcium current I_T. *A*: kinetics of deinactivation was determined by varying the length of the conditioning step to −100 mV from 100 ms to 1 s and measuring the inward current produced at the beginning of a subsequent command step to −50 mV. An example of the inward currents evoked at the beginning of the second step is shown in the box on the *bottom right*. Normalized response was plotted as a function of the duration of the conditioning step and revealed a deinactivation time constant ($\tau_{deinact}$) of 208.05 ms. *B*: kinetics of inactivation was determined by varying the interval between fixed-amplitude conditioning step to −90 mV and command step to −50 mV. Interval was increased from 15 to 555 ms in 60-ms increments. An example of the inward currents evoked at the beginning of the second step is shown in the box on the *bottom right*. Normalized response was plotted as a function of the duration of the conditioning step and revealed a inactivation time constant (τ_{inact}) of 56.1 ms.

EXPRESSION OF THE TRANSIENT VOLTAGE-DEPENDENT POTASSIUM CURRENT (I_A). In response to depolarizing current injection at, or near, threshold for action potential generation most Type III neurons showed a marked delay in the time to onset of the first spike (see Fig. 2*A*). Similar delays in action potential firing have been reported in neurons from diverse regions of the CNS as resulting, in part, from activation of the rapidly inactivating outward potassium current I_A (Burdakov and Ashcroft 2002; Varga et al. 2004).

Consequently, we next examined the relative expression of I_A-like currents in $BNST_{ALG}$ neurons. Surprisingly, an I_A-like current was observed in all of the neurons examined ($n = 19$) and was not restricted to the 16% of neurons that might be expected if it was expressed only by Type III neurons.

Like I_T channels, I_A channels require a period of membrane hyperpolarization to remove channel inactivation before they can activate. Consequently, to examine the expression of I_A-like currents in $BNST_{ALG}$ neurons we used dual-step protocols similar to those used to isolate I_T (outlined earlier). Because I_A channels are reported to deinactivate at more depolarized potentials than I_T (Burdakov and Ashcroft 2002; Varga et al. 2004) we minimized any potential contamination by I_T by conducting these studies at a holding potential of −40 mV because, at this potential, I_T channels are thought to be fully inactivated. In addition, these experiments were conducted using a modified ACSF supplemented with ZD7228 (60 μM) and $NiCl_2$ (500 μM), to block I_h and I_T, respectively.

We first examined the activation properties of I_A-like currents in $BNST_{ALG}$ neurons using a transient (500-ms) hyperpolarizing prepulse to −100 mV followed by depolarizing step commands of increasing amplitude (Fig. 7*A*). In all neurons examined, this protocol elicited a transient outward current that peaked within about 20 ms of the onset of the depolarizing step command, and which rapidly decreased in amplitude thereafter. When the resultant series of outward currents were normalized and fit with a Boltzmann equation, the I_A-like current was seen to activate at membrane potentials significantly more depolarized than that observed for I_T (~−40 mV), have a half-maximal activation potential ($V_{1/2}$) of −3.1 ± 2.7 mV, and a slope factor of 10.1 ± 0.96 mV ($n = 10$). Significantly, the I_A-like current was markedly suppressed by addition of 4-aminopyridine (4-AP; 5 mM) to the ACSF [$F(4,102) = 338.8$, $P < 0.05$], suggesting that the transient outward current was indeed mediated by activation of I_A channels (Fig. 7*A*, *inset*).

Similar to the I_T current, the rate of rise of the I_A current increased with increasing depolarizing step commands, such that the time-to-peak current was 17.1 ± 2.3 ms for depolarization steps to −30 mV and 8.1 ± 0.8 ms for depolarization steps to +5 mV. This voltage dependency is consistent with

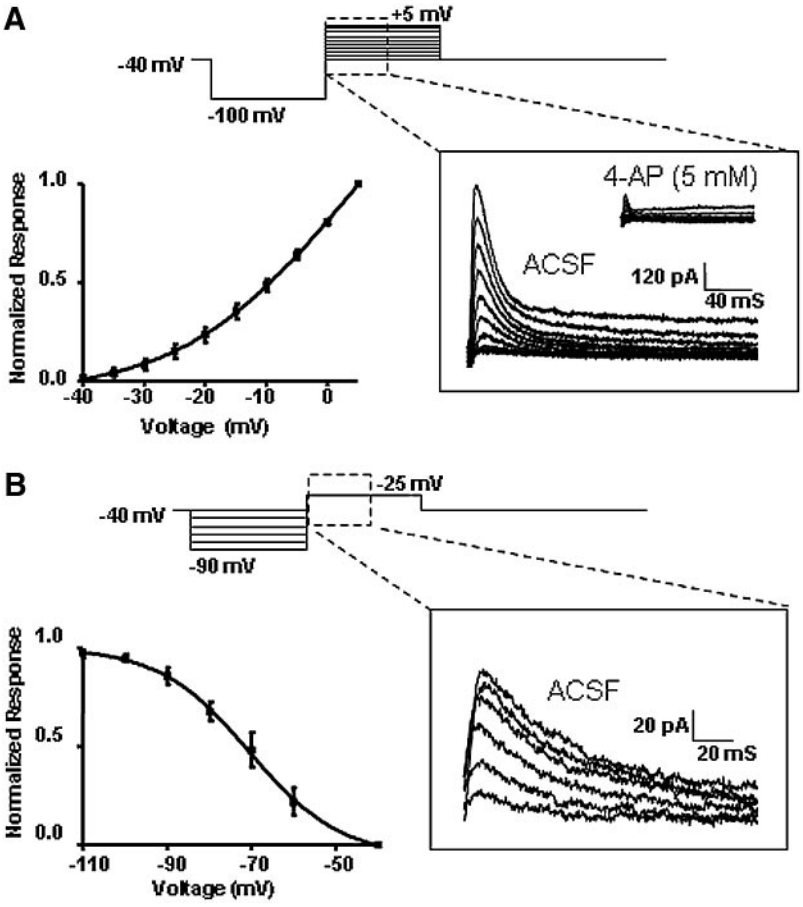

FIG. 7. $BNST_{ALG}$ neurons exhibit a transient outward current that resembled the voltage-dependent potassium current I_A. *A*, *top trace*: dual-step protocol used to determine the activation curve for the voltage-dependent potassium current I_A. An example of the outward currents evoked at the beginning of the second step is shown in the box on the *bottom right*, and this current was completely blocked in the I_A channel blocker 4-aminopyridine (4-AP, 5 mM, *inset*). Activation curve of the normalized response plotted as a function of command voltage revealed a $V_{1/2}$ of -3.1 ± 2.7 mV. *B*, *top trace*: dual-step protocol used to determine the deinactivation curve for the voltage-dependent potassium current I_A. An example of the outward currents evoked at the beginning of the second step is shown in the box on the *bottom right*. Deinactivation curve of the normalized response plotted as a function of the conditioning voltage revealed a $V_{1/2}$ of -70.4 ± 2.4 mV.

previous reports of I_A currents in other regions (Locke and Nerbonne 1997).

At a holding potential of -40 mV, the decay phase of the I_A current was best fit by a second-order exponential equation with two significantly different rates of decay ($t = 11.0$, $P < 0.05$), suggesting that I_A channels in $BNST_{ALG}$ neurons might be heteromers of different I_A channel subunits. The fast decay had a time constant for deactivation (fast τ_A) of 21.4 ± 1.2 ms ($n = 7$) and a slow decay time constant (slow τ_A) of 183.5 ± 16.1 ms ($n = 7$). Interestingly, the fast τ_A was voltage sensitive, whereby fast τ_A decreased from 22.2 ± 5.5 ms with steps to -35 mV to 14.8 ± 3.3 ms with steps to $+5$ mV. In contrast, the slow τ_A appeared to be voltage independent, such that with steps to -35 mV the slow τ_A was 187.0 ± 28.6 ms and to $+5$ mV the slow τ_A was 178.8 ± 58.3 ms.

We next investigated the voltage dependency of I_A deinactivation using a dual-step protocol similar to that outlined earlier for the deinactivation of I_T (Fig. 7*B*). As expected, the amplitude of the I_A current increased with increasing levels of prepulse hyperpolarization (Fig. 7*B*). A plot of the normalized I_A current amplitude as a function of the prepulse potential was fit with a Boltzmann equation and revealed that I_A channels in $BNST_{ALG}$ neurons were half-maximally deinactivated ($V_{1/2}$) at -70.4 ± 2.4 mV ($n = 4$), with a slope factor of -10.8 ± 2.6 mV.

We next examined whether the deinactivation and inactivation kinetics of the I_A current showed a temporal profile similar to that of I_T using protocols similar to those outlined earlier. As illustrated in Fig. 8*A*, I_A amplitude increased with increasing duration of the hyperpolarizing prepulse and showed an *e*-fold (2.13) increase ($\tau_{deinact}$) with hyperpolarizing steps of 34.6 ms ($n = 10$). We then determined the temporal domain for the inactivation kinetics (τ_{inact}) of I_A. Here the interval between the hyperpolarizing prepulse and the depolarizing step command was incrementally increased and the resultant I_A current normalized and plotted as a function of the interval duration. As illustrated in Fig. 8*B*, I_A showed an *e*-fold decrement in amplitude with a τ_{inact} of 211.41 ms ($n = 4$). In $BNST_{ALG}$ neurons deinactivation of I_A channels occurs sevenfold faster than deactivation and thus in Type I and Type III neurons, which do not express I_T, the response to inhibitory synaptic input would tend to be enhanced.

EXPRESSION OF THE INWARDLY RECTIFYING POTASSIUM CURRENT [$I_{K(IR)}$]. As illustrated in Fig. 2*B*, Type III neurons show a rapid and dramatic decrease in the voltage excursion evoked by transient hyperpolarizing current injection of increasing amplitude. This voltage-dependent and time-independent decrease in input resistance was similar to the fast rectification reported in other brain regions that is mediated by activation of an inwardly rectifying potassium current $I_{K(IR)}$ (De Jeu et al. 2002; Nisenbaum and Wilson 1995). Activation of $I_{K(IR)}$ channels is thought to play a pivotal role in the maintenance of the resting membrane potential, as well as regulating action potential duration (for review, see Nichols and Lopatin 1997). Significantly, both the fast anomalous rectification (Fig. 9*A*) and the underlying increase in membrane conductance observed in $BNST_{ALG}$ neurons (Fig. 9*B*) were blocked by addition of the

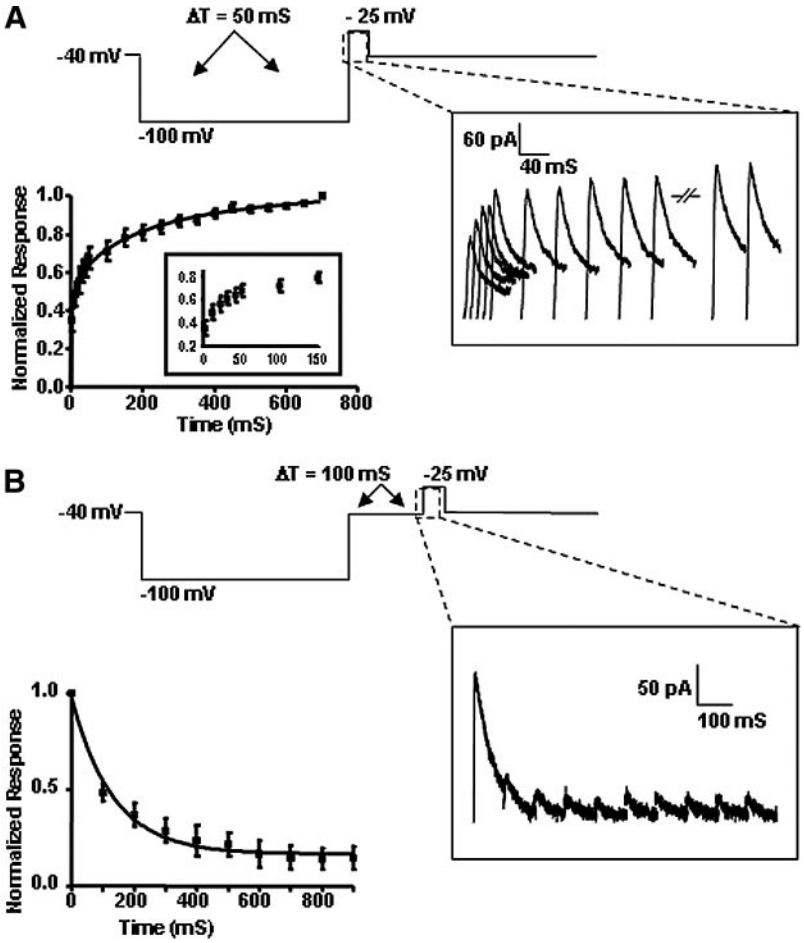

FIG. 8. Deinactivation and inactivation kinetics of I_A in $BNST_{ALG}$ neurons. *A*: kinetics of deinactivation was determined by varying the length of the conditioning step to −100 mV from 10 to 700 ms and measuring the outward current produced at the beginning of a subsequent command step to −25 mV. An example of the outward currents evoked at the beginning of the second step is shown in the box on the *bottom right*. Normalized response was plotted as a function of the duration of the conditioning step and revealed a $\tau_{deinact}$ of 34.6 ms. *B*: kinetics of inactivation was determined by varying the interval between fixed-amplitude conditioning step to −100 mV and command step to −25 mV. Interval was increased from 0 to 900 ms in 100 ms increments. An example of the outward currents evoked at the beginning of the second step is shown in the box on the *bottom right*. Normalized response was plotted as a function of the duration of the conditioning step and revealed a τ_{inact} of 211.41 ms.

nonselective K_{IR} blocker, barium chloride ($BaCl_2$, 500 μM), to the ASCF. At a holding potential of −60 mV, application of $BaCl_2$ elicited a 6.9 ± 1.1 mV ($n = 22$) depolarizing shift in the membrane potential of $BNST_{ALG}$ neurons that was associated with a 138 ± 5.0% increase in R_m (from 425.2 ± 41.2 to 557.3 ± 49.9 MΩ) and a 133.6 ± 9.5% increase in τ_m. In voltage clamp, the depolarization was seen to be mediated by a 16.6 ± 5.4 pA ($n = 9$) inward current and had a reversal potential of −74.2 ± 2.0 mV. Thus $I_{K(IR)}$ channels appear to play a significant role in regulating the resting membrane potential of Type III neurons. It is noteworthy that in several Type III neurons, blockade of $I_{K(IR)}$ channels with $BaCl_2$ unmasked a small, time-dependent, inward current indicative of the presence of I_h (see Fig. 9*A*).

EXPRESSION OF THE PERSISTENT SODIUM CURRENT (I_{NaP}). While examining the properties of single action potentials in $BNST_{ALG}$ neurons it was noted that transient (10 ms), subthreshold, depolarizing current injection could elicit a voltage response whose decay far outlasted the normal time constant for membrane discharge. Similar slow depolarizing potentials have been observed in neurons of the entorhinal cortex and hippocampus (Saraga and Skinner 2002), where they were attributed to the activation of a slowly inactivating persistent sodium current (I_{NaP}). Consequently, we next examined $BNST_{ALG}$ neurons for the presence of the persistent sodium current (I_{NaP}). These experiments were conducted using a modified ACSF that contained potassium and calcium channel blockers, as well as a reduced sodium concentration to prevent contamination by all-or-none action potentials (see METHODS). The presence of I_{NaP} was probed using a voltage-ramp protocol in which the command voltage was ramped from −100 to +10 mV at a rate of 10 mV/s. In all $BNST_{ALG}$ neurons tested ($n = 14$), the slow voltage-ramp protocol elicited a robust inward current (Fig. 9*C*) that activated at membrane potentials more positive than −50 mV, reached a peak at −27.5 ± 2.2 mV, and had a half-maximal activation potential ($V_{1/2}$) of −39.4 ± 1.8 mV. In all cases the inward current was completely blocked by the sodium channel blocker TTX (1 μM, $n = 6$, Fig. 9*C*), and was significantly attenuated (74%) by addition of the nonselective I_{NaP} channel blocker riluzole (30 μM) to the ACSF ($t = 5.93$, $P < 0.05$; data not shown). These data suggest that, like I_A channels, I_{NaP} channels are ubiquitously expressed in $BNST_{ALG}$ neurons.

DISCUSSION

Identification of distinct physiological cell types within the $BNST_{ALG}$

Previous studies in the $BNST_{ALG}$ have suggested the existence of distinct neuronal subpopulations that differ in their cytoarchitecture, chemoarchitecture, and projection patterns. Here, we provide additional evidence for three physiologically distinct subpopulations of $BNST_{ALG}$ neurons that can be categorized according to their response to hyperpolarizing and

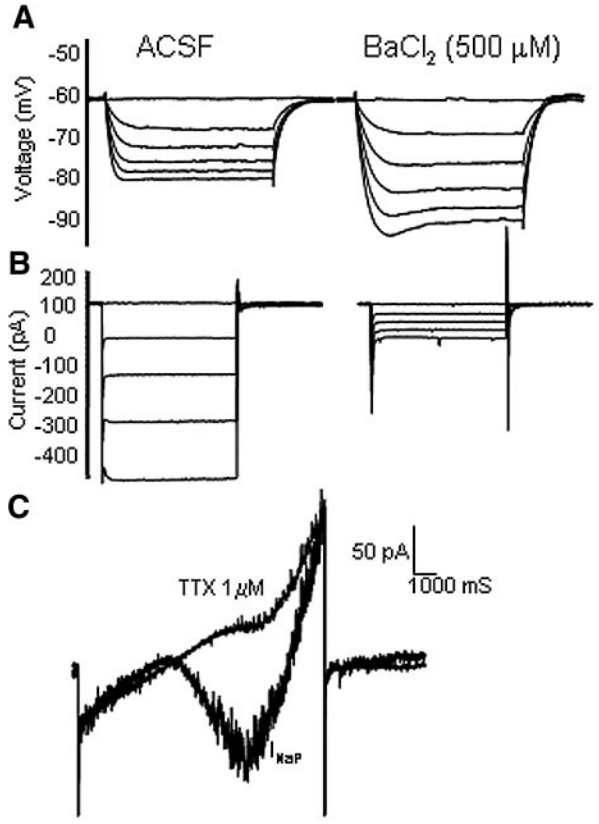

FIG. 9. $BNST_{ALG}$ neurons exhibit an inwardly rectifying potassium current, $I_{K(IR)}$, and a persistent inward sodium current, I_{NaP}. *A*: voltage response to hyperpolarizing current in a representative Type III neuron before and during application of the $I_{K(IR)}$ channel blocker $BaCl_2$. *B*: current response to hyperpolarizing voltage steps in voltage-clamp mode in a representative Type III neuron. $BaCl_2$ (500 μM) blocked the $I_{K(IR)}$ current. *C*: a representative example of the I_{NaP} current recorded from a $BNST_{ALG}$ neuron. In response to a command voltage that ramped from 100 to +10 mV at a rate of 10 mV/s, a large inward current was observed with a $V_{1/2}$ of -39.4 ± 1.8 mV. This inward current was blocked by the sodium channel blocker tetrodotoxin (TTX, 1 μM).

depolarizing current injection. Furthermore, we extend these observations to show that the differential expression of at least five intrinsic membrane currents shapes the response of each cell type, thus dictating their input–output relationship.

In our initial study on the properties of cells in the medial and lateral BNST (Rainnie 1999), we reported that neurons in these two regions could be differentiated by their relative expression of a depolarizing sag in the voltage response to hyperpolarizing current injection, which was thought to be mediated by the hyperpolarization-activated cation conductance I_h, as well as a transient depolarizing potential that was thought to be mediated by the low-threshold calcium current I_T. These observations were subsequently confirmed in mice in a more detailed study by Egli and Winder (2003), who further reported that some BNST neurons also exhibit a fast inward rectification in the voltage response to hyperpolarizing current injection (Egli and Winder 2003). However, these were predominantly current-clamp studies and thus the underlying intrinsic membrane currents were not characterized beyond establishing their presence in BNST neurons. Consequently, it was unclear whether BNST neurons exhibit varying levels of the same intrinsic currents or whether distinct physiological subtypes of neurons exist within the BNST.

Here, we used a simple visual discrimination of the current-clamp traces recorded from 276 $BNST_{ALG}$ neurons to provisionally divide this cell population into three distinct physiological cell types. The criteria used for the discrimination were based solely on the shape of the voltage response to hyperpolarizing and depolarizing current injection (see Fig. 2, *A* and *B*). Thus Type I neurons expressed a depolarizing sag in response to hyperpolarizing current injection, but did not exhibit any signs of low-threshold spiking or burst-firing activity. Type II neurons expressed the depolarizing sag and also exhibited robust rebound spiking and/or burst-firing activity. Type III neurons exhibited a pronounced fast inward rectification to hyperpolarizing current injection and did not exhibit any signs of low-threshold spiking or burst-firing activity. Interestingly, a similar distribution of BNST neurons expressing these characteristics has been reported in mice (Egli and Winder 2003), suggesting that these three physiological cell types are not species specific.

Based on the criteria outlined earlier, we reasoned that the three subtypes of $BNST_{ALG}$ neuron would differentially express one or more of at least three intrinsic membrane currents: I_h, I_T, and $I_{K(IR)}$. Neurons of the central nucleus of the amygdala (CeA), a GABAergic homologue of the $BNST_{ALG}$ (for review, see Alheid 2003), have also been subdivided into at least three cell types based primarily on their action potential firing patterns (Martina et al. 1999). Significantly, the firing pattern of each subtype was differentially modulated by application of the I_A-channel blocker 4-AP or the I_T-channel blocker $NiCl_2$, suggesting that distinct subtypes of neurons in this BNST homologue can also be differentiated based on their expression of intrinsic membrane currents.

The discussion below outlines the properties for each of the currents expressed by $BNST_{ALG}$ neurons and is followed by a brief discussion of how these currents work in concert to shape the characteristic response profiles of the different $BNST_{ALG}$ cell types and the potential significance of physiological diversity.

Hyperpolarization-activated nonspecific cation current (I_h)

The hyperpolarization-activated cyclic nucleotide gated current I_h is a mixed cation current that activates at membrane potentials more negative than -50 mV, has a half-maximal activation voltage ($V_{1/2}$) that ranges between -60 and -90 mV, and is blocked by external application of either CsCl or ZD7288 (for review, see Robinson and Siegelbaum 2003). $BNST_{ALG}$ neurons exhibited a voltage- and time-dependent inward current with similar physiological and pharmacological properties such that the inward current deinactivated at potentials below -50 mV (Fig. 4*C*), had a $V_{1/2}$ of about -80 mV, and was blocked by both 5 mM CsCl and 30 μM ZD7288. Significantly, pharmacological blockade of I_h channels in $BNST_{ALG}$ neurons resulted in a net hyperpolarizing shift in the resting membrane potential (about -60 to -64.2 mV), which was associated with a significant increase in the membrane input resistance (161.6%). Thus in Type I and Type II $BNST_{ALG}$ neurons, I_h plays a significant role in regulating both the resting membrane potential and the resting membrane input resistance.

Four genes (HCN1–HCN4) encode distinct isoforms of the I_h channel. The BNST has high expression levels of HCN1

mRNA, moderate levels of HCN3, and low levels of HCN2 and HCN4 mRNA (Monteggia et al. 2000). Importantly, each of these isoforms differs in its kinetics, voltage dependency, and sensitivity to cyclic adenosine monophosphate (cAMP) modulation (for review, see Robinson and Siegelbaum 2003). Thus HCN3 channels activate more slowly than HCN2 channels, which in turn activate more slowly than HCN1 channels (Altomare et al. 2003; Mistrik et al. 2005). Moreover, HCN isoforms have been shown to coassemble into functional heteromers and form I_h channels with properties that are often intermediate between their constituent homomers (Chen et al. 2001).

$BNST_{ALG}$ neurons could be subdivided into two populations with either slow or fast I_h activation kinetics, which may reflect differences in the subunit composition of the I_h channels in Type I and Type II $BNST_{ALG}$ neurons. The mean activation rate of the faster group (110 ms) is similar to the activation kinetics reported for homomeric HCN1 channels (Santoro et al. 2000), whereas the mean rate for the slower group (173 ms) suggested the presence of heteromeric I_h channels that may contain HCN1 subunits in association with one or more subunits of HCN2–HCN4. Evidence from in situ hybridization studies (ibid) would suggest that heteromeric channels of the slower group would consist of HCN1 and HCN3 subunits. Consistent with this hypothesis, using single-cell RT-PCR analysis of the mRNA from recorded $BNST_{ALG}$ neurons we have found neurons that contain mRNA only for HCN1, or both HCN1 and HCN3, and rarely HCN2 or HCN4 (Hammack et al. 2006). Moreover, I_h channels formed from heteromers of HCN1/HCN4 have much slower activation kinetics (>5 s; Altomare et al. 2003) than that observed in $BNST_{ALG}$ neurons and thus are unlikely to mediate I_h currents in the $BNST_{ALG}$.

Significantly, the different HCN isoforms also differ in the degree to which they can be modulated by cAMP. For example, cAMP has minimal effect on HCN1 channel activity (Santoro et al. 1998), strongly augments HCN2 channel activity (Ludwig et al. 1998), and inhibits HCN3 channel activity (Mistrik et al. 2005). We have shown that $BNST_{ALG}$ neurons can be subdivided into two distinct groups based on their fast versus slow I_h activation kinetics. The different I_h kinetics most likely reflect differences in the channel subunit composition, and thus cAMP may differentially modulate I_h activity in these two cell populations. Consequently, any receptor–effector complex that activates the cAMP second-messenger cascade would be expected to differentially regulate the excitability of $BNST_{ALG}$ neurons. In the CNS, I_h channel activity is enhanced by serotonin (Cardenas et al. 1999), dopamine (Wu and Hablitz 2005), and corticotropin-releasing factor (CRF; Qiu et al. 2005), all of which are released into the $BNST_{ALG}$ during exposure to a stressor or novel environments. Thus local release of neurotransmitters in response to stressors, novelty, drugs of abuse, or goal-directed behaviors might promote I_h-mediated activity in select subtypes of $BNST_{ALG}$ neurons.

Low-threshold calcium current (I_T)

In our first BNST paper (Rainnie 1999; see also Egli and Winder 2003), we suggested that neurons in the lateral BNST express a low-threshold I_T-like calcium current. However, this study did not examine either the properties of the I_T-like current or its relative distribution across cell types. Here, we expand on these original observations to show that an I_T current does in fact mediate burst-firing activity in the $BNST_{ALG}$, but only in Type II neurons.

Thus Type II neurons showed a transient inward current that decayed rapidly (τ = 20 ms), had $V_{1/2}$ of activation of −50 mV, a $V_{1/2}$ of deinactivation of −77.6 mV, and a mean amplitude of −102 pA in response to step commands from −90 to −40 mV. These properties are consistent with those previously reported for I_T in several other brain regions (see Perez-Reyes 2003). Moreover, the transient inward current was significantly attenuated by the relatively selective T-type calcium channel blockers $NiCl_2$ (500 μM) and mibefradil (10 μM).

Calcium channels are complex proteins composed of four or five distinct subunits in which the α1 subunit contains the pore-forming core (for review, see Catterall 2000). To date a family of ≥10 subunit genes have been identified and cloned. Three α-subunits that form calcium channels with properties similar to those of I_T have been cloned and named α1G, α1H, and α1I (Perez-Reyes 2003). Of these three subunits, in situ hybridization studies have shown moderate to high levels for α1G and α1H mRNA in the $BNST_{ALG}$ (Talley et al. 1999). Although the voltage dependencies of these three α-subunits are similar, they have significantly different kinetics and sensitivity to blockers (Lee et al. 1999). Thus I_T channels incorporating the α1I subunit have slower inactivation (137 ms) kinetics than those containing α1G or α1H (Klockner et al. 1999). Consistent with the in situ hybridization studies (ibid), the relatively rapid inactivation kinetics reported here for I_T in $BNST_{ALG}$ neurons suggests that these channels may incorporate either the α1G and/or α1H subunits. Although α1G subunits are 24-fold less sensitive than α1H sensitivities to blockade by $NiCl_2$ (Lee et al. 1999), the concentration used in the present study (500 μM) could not differentiate the subunit composition of I_T in $BNST_{ALG}$ neurons.

Several neurotransmitters have been shown to modulate I_T channel function including 5-HT (Fraser and MacVicar 1991), acetylcholine (Fisher and Johnston 1990), substance P (Ryu and Randic 1990), estrogen (Qiu et al. 2006), catecholamines (Marchetti et al. 1986), and angiotensin II (Buisson et al. 1992). All of these neurotransmitters are released in the BNST and thus might regulate I_T functioning in Type II neurons. Intriguingly, 5-HT has been shown to inhibit I_T by 5-HT_2 receptor activation (Placantonakis et al. 2000), whereas 5-HT_7 receptor activation has been reported to increase I_T (Lenglet et al. 2002). Both 5-HT_2 and 5-HT_7 receptors are functionally expressed in $BNST_{ALG}$ neurons (Hammack et al. 2005) and it remains to be determined whether activation of either of these two receptors subtypes can modulate I_T in Type II neurons.

Voltage-dependent potassium current (I_A)

Significantly, all three subtypes of $BNST_{ALG}$ neuron expressed an I_A-like current. Consistent with the description of I_A elsewhere in the brain, the I_A current in $BNST_{ALG}$ neurons exhibited marked voltage dependency and had a $V_{1/2}$ of activation of −3.1 mV, a $V_{1/2}$ of deinactivation of −70 mV, and a mean current of 612 pA following voltage steps from −100 to 0 mV (for review, see Rudy 1988). However, although the threshold for activation (>−40 mV) was similar to that reported in several brain regions (see Burdakov and Ashcroft

2002), it was more positive than that in others (Locke and Nerbonne 1997).

Native I_A channels are made up of the gene products of several members of the Kv potassium channel family: Kv1.4, Kv 3.3, Kv3.4, and the Kv4 family of subunits. Importantly, each Kv subunit has distinct activation and inactivation kinetics as well as differential sensitivity to pharmacological blockers (for review, see Robertson 1997). Three of these subunits—Kv1.4, Kv4.2, and Kv4.3—have been detected in the $BNST_{ALG}$ (Serodio and Rudy 1998). It is noteworthy that the activation and deinactivation properties of Kv4.3 are similar to the values reported here for I_A in $BNST_{ALG}$ neurons (Tsaur et al. 1997), suggesting that these neurons may express a common Kv channel subunit. Consistent with this hypothesis, the inactivation decay of I_A was best fit by a dual-exponential having both a fast ($\tau = 21$ ms) and a slow time constant ($\tau = 184$ ms), and a similar biexponential function has been reported elsewhere for Kv4.3 subunits (Franqueza et al. 1999). Intriguingly, Kv4.1 and Kv4.2 are thought to be localized to the somatodendritic compartment (Song 2002) and are blocked by high extracellular 4-AP (5 mM), much like the I_A current observed in $BNST_{ALG}$ neurons. In contrast, Kv1.4 subunits are localized to the axonal compartment and sensitive to low micromolar concentrations of 4-AP (for review, see Gutman et al. 2005). Thus members of the Kv4 family of subunits may regulate somatic excitability of $BNST_{ALG}$ neurons, whereas channels containing the Kv1.4 subunit may modulate dendritic excitability.

As discussed in the following text, in Type II $BNST_{ALG}$ neurons I_A acts to attenuate I_T and thus regulate burst-firing activity in these neurons. Like I_T, several neurotransmitters have been shown to modulate I_A channel function including 5-HT (Farley and Auerbach 1986), acetylcholine (Nakajima et al. 1986), norepinephrine (Aghajanian 1985), and cholecystokinin (Burdakov and Ashcroft 2002). Significantly, many of the same neurotransmitters that can increase I_T (i.e., 5-HT and acetylcholine) also act to inhibit I_A. As discussed below, such a combination of effects would dramatically enhance burst firing in Type II $BNST_{ALG}$ neurons.

Inwardly rectifying potassium current [$I_{K(IR)}$]

In current-clamp mode, many $BNST_{ALG}$ neurons expressed a type of fast anomalous rectification that was most apparent in Type III neurons (see Fig. 2). In voltage clamp, the fast anomalous rectification was associated with a voltage-dependent increase in membrane conductance that was blocked by addition of 500 μM $BaCl_2$ to the ACSF, consistent with its being mediated by activation of an inwardly rectifying potassium current $I_{K(IR)}$.

Seven subfamilies of $I_{K(IR)}$ channel have been cloned (K_{ir1-7}) (Dascal et al. 1993; Ho et al. 1993), which can be distinguished based on their rectification properties and their regulation by intracellular messengers (for review, see Stanfield et al. 1994). K_{ir} channels are tetramers with a unique two-transmembrane domain structure (see Nichols and Lopatin 1997). Significantly, members of the $K_{ir}2.0$ subfamily are constitutively active, blocked by barium, and found predominantly in the brain, where these channels are thought to play a major role in clamping the resting membrane potential close to the reversal potential for potassium (Nichols and Lopatin 1997). These data are consistent with the observation that Type III neurons have a lower resting membrane potential compared with that of Type I and Type II neurons (see Table 1). Moreover, $K_{ir}2.3$ channels are reported to localize in the dendrites (Day et al. 2005) and postsynaptic membranes of cortical pyramidal neurons (Inanobe et al. 2002), where they are thought to regulate excitatory transmission (Takigawa and Alzheimer 2002). Thus in Type III $BNST_{ALG}$ neurons $I_{K(IR)}$ channels may also function to regulate excitatory afferent input.

However, $BaCl_2$ induced a membrane depolarization and increased the input resistance of all neurons tested (data not shown), suggesting that $I_{K(IR)}$ channels are ubiquitously expressed in $BNST_{ALG}$ neurons but that the relative number and/or subunit composition varies from cell type to cell type. Thus subpopulations of $BNST_{ALG}$ neurons may express unique combinations of K_{ir} subunits. Consistent with this hypothesis, using RT-PCR we have detected mRNA for $K_{ir}2.1$ and $K_{ir}2.3$ subunits in isolated sections of the BNST (Hammack et al. 2006; but see Karschin et al. 1996). Moreover, $K_{ir}2.1$–$K_{ir}2.4$ subunits combine to form homo- and heteromeric tetramers with different biophysical properties and differential subunit composition may explain the variability in $I_{K(IR)}$ channel properties observed in neurons both between and within different brain nuclei (see Isomoto et al. 1997).

It should be noted, however, that in the suprachiasmatic nucleus $BaCl_2$ induced a membrane depolarization that was attenuated by blockade of the ether a go-go potassium channel eag2 (De Jeu et al. 2002). It remains to be determined what contribution, if any, eag2 channels may play in regulating the activity of $BNST_{ALG}$ neurons.

Persistent sodium current (I_{NaP})

All $BNST_{ALG}$ neurons examined displayed a TTX- and riluzole-sensitive inward current that activated at subthreshold membrane potentials (−50 mV), had a half-maximal activation at −39 mV, and peaked at −28 mV. These properties are similar to those of I_{NaP} reported in the cortex (Maurice et al. 2001; Urbani and Belluzzi 2000), but were slightly more depolarized than reports of I_{NaP} in other brain regions (Gorelova and Yang 2000).

Of the ten subfamilies of sodium channels that have been identified to date ($Na_v1.1$–$Na_v1.9$ and Na_x), only $Na_v1.1$, $Na_v1.2$, $Na_v1.3$, and $Na_v1.6$ are expressed at high levels in the CNS (Goldin 2001). Significantly, the expression of Nav1.5 is restricted to the limbic regions of the brain, including the BNST (Hartmann et al. 1999). Moreover, $Na_v1.5$ channel subunits are pharmacologically distinct from other subunits in that they are inhibited by micromolar concentrations of TTX, as opposed to nanomolar concentrations. Thus activation of sodium channels containing the $Na_v1.5$ subunit may contribute to the expression of I_{NaP} in $BNST_{ALG}$ neurons. In cerebellar Purkinje cells, I_{NaP} is thought to be mediated by the $Na_v1.6$ α-subunit (Vega-Saenz de Miera et al. 1997). However, neurons of the sensorimotor cortex show layer-specific differences in the properties of I_{NaP} (Aracri et al. 2006), suggesting that I_{NaP} channels may show region-specific subunit composition.

Noninactivating I_{NaP} currents have been observed in a variety of brain regions, where they participate in the regulation of burst-firing activity (Stafstrom et al. 1985), the control of

membrane excitability (Wu et al. 2005), subthreshold membrane potential oscillations (Agrawal et al. 2001), and in the amplification of excitatory postsynaptic potentials in distal dendrites (Crill 1996). Interestingly, 5-HT is reported to enhance I_{NaP} currents (Carr et al. 2002), possibly by activation of 5-HT_2 receptors (Harvey et al. 2006). We have shown that 5-HT excites a subpopulation of $BNST_{ALG}$ neurons by activation of postsynaptic 5-HT_2 receptors (Hammack et al. 2005). It remains to be determined whether an enhancement of the I_{NaP} current contributes to the excitatory action of 5-HT and whether this action is cell type specific.

Functional relevance of multiple physiological cell types

Although there is some discussion about the merits of neural taxonomy (Nelson 2002), categorization of discrete cell types based on their intrinsic membrane currents, as outlined here, has been successfully applied to multiple subcortical structures including the inferior colliculus (Peruzzi et al. 2000), the hypothalamic paraventricular nucleus (Boudaba et al. 1996), the lateral geniculate nucleus (Kaneda and Kaneko 1991), and the central nucleus of the amygdala (Martina et al. 1999). Moreover, although we did not present gene expression data here, our preliminary single-cell RT-PCR data support the premise of distinct categories of $BNST_{ALG}$ neurons based on their differential expression of genes encoding selective ion channels (Hammack et al. 2006). It should be noted, however, that currents that were not examined here may also play an equal role in shaping the input–output response of the different subtypes of $BNST_{ALG}$ neurons. Nevertheless, in this study we have defined five elementary intrinsic membrane currents whose relative expression confers on the three $BNST_{ALG}$ neuron subtypes many of their functional attributes.

Thus Type I neurons constitute 29% of all $BNST_{ALG}$ neurons and express I_h, I_A, I_{NaP}, and to a lesser extent $I_{K(IR)}$. In these cells, I_h was activated at voltages close to rest and played a significant role in regulating the resting membrane potential and membrane input resistance. Moreover, activation of I_h produced a rebound excitation after inhibitory voltage excursions, suggesting that this current may also contribute to intrinsic membrane oscillations in Type I $BNST_{ALG}$ neurons. Type I neurons also express I_{NaP}, which has been shown to contribute to subthreshold membrane potential oscillations in neocortical neurons (Alonso and Llinas 1989; Amitai 1994), and amplify theta-frequency oscillations in subicular neurons (Wang et al. 2006).

However, Type I neurons also express I_A channels and thus the extent of any membrane oscillation would be determined by the relative interaction between I_A, I_h, and I_{NaP}. Expression of I_A may also contribute to the regular firing pattern observed in $BNST_{ALG}$ neurons. Because the majority of these neurons are thought to be GABAergic (Sun and Cassell 1993), the regular firing pattern of Type I neurons would be expected to evoke tonic γ-aminobutyric acid (GABA) release, rather than the release of peptide cotransmitters, as might be expected from burst-firing Type II $BNST_{ALG}$ neurons (see following text).

Type II neurons constitute 55% of all $BNST_{ALG}$ neurons and most likely represent a significant proportion of $BNST_{ALG}$ output neurons. Type II neurons were distinguished from Type I neurons only by their robust expression of the I_T current. Nevertheless, the addition of this single current to their repertoire had a significant impact on the functional properties of Type II neurons compared with Type I neurons. In Type II $BNST_{ALG}$ neurons, the rebound excitation after an inhibitory voltage excursion was markedly enhanced when compared with the rebound excitation observed in Type I $BNST_{ALG}$ neurons, suggesting that I_T and I_h would act synergistically to facilitate oscillatory burst firing in Type II $BNST_{ALG}$ neurons. Type II neurons also expressed a prominent I_{NaP}, further suggesting that these neurons would show a propensity for oscillatory burst-firing activity. Interestingly, I_T has been shown to act in concert with I_h to promote rhythmic burst firing in thalamocortical relay neurons during slow-wave sleep, and changes in the rhythmicity of these neurons have been argued to underlie sleep and vigilance (for review, see Llinas and Steriade 2006).

Because of an overlap in their kinetics of activation and deinactivation, the expression of I_T is tightly regulated by I_A in Type II neurons. However, the $V_{1/2}$ for activation of I_A is more depolarized than I_T and thus I_T would be preferentially activated with membrane depolarization at or near rest. Subsequent depolarization would activate I_A and begin to shunt I_T, thus setting a temporal constraint on the duration of I_T-induced burst firing. Thus any factor that could attenuate I_A would be expected to dramatically enhance burst-firing activity in Type II neurons. High-frequency burst-firing activity is thought to promote the release of peptide neurotransmitters from hippocampal GABAergic neurons (Baraban and Tallent 2004). A significant proportion of GABAergic output neurons in the $BNST_{ALG}$ coexpress neuropeptides, including vasoactive intestinal polypeptide, cholecystokinin, substance P, neurotensin, CRF, and methionine-enkephalin (Woodhams et al. 1983). Consequently, the transition from tonic to burst-firing activity in Type II neurons might signal a transition from GABA release to neuropeptide release in target structures of Type II $BNST_{ALG}$ neurons. Behaviorally, alternating between tonic and burst-firing activity in Type II neurons may signal changes in anxiety-like states in a manner similar to that proposed for thalamocortical neurons in the behavioral state transition from sleep to wakefulness (Llinas and Steriade 2006).

Type III neurons represent 16% of the total cell population and were distinguishable from Type I and Type II neurons by their prominent expression of $I_{K(IR)}$. Consistent with this observation, Type III neurons had a more hyperpolarized resting membrane potential and a higher threshold for firing action potential generation than did Type I and Type II neurons. Consequently, Type III neurons would require a stronger excitatory input to reach threshold for action potential generation than either Type I or Type II neurons. Moreover, Type III neurons express an I_A current and the more hyperpolarized resting membrane potential of these neurons ensures that the probability of I_A deinactivation at rest is greater than that in Type I and Type II neurons. Thus any excitatory input would also have to overcome I_A activation before pushing the membrane potential past threshold for action potential generation. These properties are reflected in the long latency to firing displayed by Type III neurons. Although Type III neurons express I_{NaP}, the lack of a prominent I_h or I_T current in these neurons would suggest that I_{NaP} most likely contributes to signal processing in the dendrites of these neurons rather than contributing to oscillatory firing activity.

Are there anatomical correlates to $BNST_{ALG}$ cell types?

At present, it is unclear whether the three cell types described here positively correlate with any other phenotypic feature such as projection pattern, neurotransmitter content, or morphological characteristics. Initial investigations into the morphological properties of biocytin-filled neurons have not, as yet, revealed differences that correlate with either the physiological cell type or their location within specific $BNST_{ALG}$ subnuclei (unpublished observation); however, a thorough analysis has yet to be completed.

Within the $BNST_{ALG}$, neurons showing the highest level of GABAergic immunoreactivity are thought to be intrinsic interneurons, although they also project to more distant regions of the central extended amygdala (Sun and Cassell 1993). However, GABAergic neurons of the $BNST_{ALG}$ also project rostrally to other forebrain regions and caudally to distal sites within the hindbrain. Indeed, a combined Golgi and electron microscopic study of the juxtacapsular nucleus revealed two basic cell types—interneurons and projection neurons—with 80% of neurons described as bipolar projection neurons (Larriva-Sahd 2004), suggesting that GABAergic neurons may function as both intrinsic interneurons and projection neurons. Interestingly, within the oval nucleus of the $BNST_{ALG}$, the most frequently observed morphological cell type (44%) was that of common spiny neurons, which were characterized by short axons that were intrinsic to the oval nucleus and thus likely modulate local network activity (Larriva-Sahd 2006). Here, we report that 55% of $BNST_{ALG}$ neurons were Type II neurons, thus raising the intriguing possibility that the majority of Type II neurons might be local-circuit intrinsic interneurons. These data also suggest that afferent input to the $BNST_{ALG}$ might preferentially target an intrinsic network of interneurons that may serve to regulate projection neurons and thus the output of the $BNST_{ALG}$.

It is noteworthy that, although most of the $BNST_{ALG}$ neurons are believed to be GABAergic (70–90%; McDonald 1983; Sun and Cassell 1993), the properties of Type III neurons most closely resemble those of neurons located in the lateral part of the ventral BNST that project to the ventral tegmental area (Dumont and Williams 2004) and are thought to be glutamatergic (Georges and Aston-Jones 2002). Indeed neurons expressing vesicular glutamate transporter 2 (Vglut2) are found in several subregions of the BNST, including the ventrolateral area (Hur and Zaborsky 2005). However, no Vglut2-containing neurons were observed in the $BNST_{ALG}$ regions dorsal to the anterior commissure.

Many GABAergic neurons of the $BNST_{ALG}$ also coexpress one or more peptide neurotransmitters (Woodhams et al. 1983). Importantly, the coexpression patterns of peptides in the $BNST_{ALG}$ can be either mutually inclusive or exclusive. For example, GABAergic $BNST_{ALG}$ neurons can coexpress CRF or methionine-enkephalin, but these peptides are never coexpressed in the same GABAergic neuron (Veinante et al. 1997). In contrast, the majority of CRF immunoreactive neurons are also immunoreactive for neurotensin (Shimada et al. 1989). As discussed earlier, burst firing in $BNST_{ALG}$ neurons would be expected to promote the release of peptide neurotransmitter rather than GABA. Because many of the $BNST_{ALG}$ neurons that coexpress peptide neurotransmitters with GABA have been shown to project to distal sites such as the locus coeruleus (Lechner and Valentino 1999) and central gray (Gray and Magnuson 1992), the valence of $BNST_{ALG}$ input to these sites could be dramatically altered depending on whether the firing pattern of the afferent $BNST_{ALG}$ neurons promotes the release of GABA, peptide, or both. We have yet to determine whether the physiological cell types described herein correlate with any particular peptidergic phenotype. The development of transgenic mice expressing fluorescent reporter genes under the regulation of gene-specific promoters (Herbison et al. 2001) will greatly assist these studies.

Similarly, $BNST_{ALG}$ neurons can display complex responses to single neurotransmitters (Egli et al. 2005; Levita et al. 2004; Rainnie 1999). For example, 5-HT can elicit one of four different response patterns in individual $BNST_{ALG}$ neurons, including an inhibitory response, an excitatory response, a mixed inhibitory and excitatory response, or no response (Levita et al. 2004; Rainnie 1999). Investigations are currently under way to determine whether a correlation exists between the 5-HT response profile and individual $BNST_{ALG}$ cell types.

In summary, these data argue for the existence of three physiological cell types within the $BNST_{ALG}$, whose response to hyperpolarizing and depolarizing current injection is shaped by the presence of several intrinsic membrane currents. These data provide the basic framework by which we can begin to build the network properties of the $BNST_{ALG}$. Because the $BNST_{ALG}$ is an important structure in regulating the behavioral response to affective stimuli, the functional mapping of networks that process this information is critical for the understanding of how this system may be altered during pathological states, including anxiety disorders and drug addiction.

ACKNOWLEDGMENTS

Present address of S. E. Hammack: University of Vermont, Department of Psychology, John Dewey Hall, 2 Colchester Avenue, Burlington, VT 05405.

GRANTS

This work was supported by Science and Technology Centers Integrative Partnership Program of the National Science Foundation (The Center for Behavioral Neuroscience) Grant IBN-987675, Yerkes National Primate Research Center Base Grant RR-00165 awarded by the Animal Resources Program of National Institutes of Health, and National Institute of Mental Health Grants MH-072908 to D. G. Rainnie and MH-072088 to S. E. Hammack.

REFERENCES

Adamec R. The relationship between the amygdala and bed nucleus of the stria terminalis in the cat: an evoked potential and single cell study. *Behav Neural Biol* 52: 295–320, 1989.

Aghajanian GK. Modulation of a transient outward current in serotonergic neurones by alpha 1-adrenoceptors. *Nature* 315: 501–503, 1985.

Agrawal N, Hamam BN, Magistretti J, Alonso A, Ragsdale DS. Persistent sodium channel activity mediates subthreshold membrane potential oscillations and low-threshold spikes in rat entorhinal cortex layer V neurons. *Neuroscience* 102: 53–64, 2001.

Alheid GF. Extended amygdala and basal forebrain. *Ann NY Acad Sci* 985: 185–205, 2003.

Alheid GF, Heimer L. New perspectives in basal forebrain organization of special relevance for neuropsychiatric disorders: the striatopallidal, amygdaloid, and corticopetal components of substantia innominata. *Neuroscience* 27: 1–39, 1988.

Alonso A, Llinas RR. Subthreshold Na^+-dependent theta-like rhythmicity in stellate cells of entorhinal cortex layer II. *Nature* 342: 175–177, 1989.

Altomare C, Terragni B, Brioschi C, Milanesi R, Pagliuca C, Viscomi C, Moroni A, Baruscotti M, DiFrancesco D. Heteromeric HCN1–HCN4 channels: a comparison with native pacemaker channels from the rabbit sinoatrial node. *J Physiol* 549: 347–359, 2003.

Amir S, Lamont EW, Robinson B, Stewart J. A circadian rhythm in the expression of PERIOD2 protein reveals a novel SCN-controlled oscillator in the oval nucleus of the bed nucleus of the stria terminalis. *J Neurosci* 24: 781–790, 2004.

Amitai Y. Membrane potential oscillations underlying firing patterns in neocortical neurons. *Neuroscience* 63: 151–161, 1994.

Aracri P, Colombo E, Mantegazza M, Scalmani P, Curia G, Avanzini G, Franceschetti S. Layer-specific properties of the persistent sodium current in sensorimotor cortex. *J Neurophysiol* 95: 3460–3468, 2006.

Arluison M, Brochier G, Vankova M, Leviel V, Villalobos J, Tramu G. Demonstration of peptidergic afferents to the bed nucleus of the stria terminalis using local injections of colchicine. A combined immunohistochemical and retrograde tracing study. *Brain Res Bull* 34: 319–337, 1994.

Aston-Jones G, Harris GC. Brain substrates for increased drug seeking during protracted withdrawal. *Neuropharmacology* 47, *Suppl.* 1: 167–179, 2004.

Baraban SC, Tallent MK. Interneuron diversity series: interneuronal neuropeptides—endogenous regulators of neuronal excitability. *Trends Neurosci* 27: 135–142, 2004.

Boudaba C, Szabo K, Tasker JG. Physiological mapping of local inhibitory inputs to the hypothalamic paraventricular nucleus. *J Neurosci* 16: 7151–7160, 1996.

Buisson B, Bottari SP, de Gasparo M, Gallo-Payet N, Payet MD. The angiotensin AT2 receptor modulates T-type calcium current in non-differentiated NG108-15 cells. *FEBS Lett* 309: 161–164, 1992.

Burdakov D, Ashcroft FM. Cholecystokinin tunes firing of an electrically distinct subset of arcuate nucleus neurons by activating A-type potassium channels. *J Neurosci* 22: 6380–6387, 2002.

Cardenas CG, Mar LP, Vysokanov AV, Arnold PB, Cardenas LM, Surmeier DJ, Scroggs RS. Serotonergic modulation of hyperpolarization-activated current in acutely isolated rat dorsal root ganglion neurons. *J Physiol* 518: 507–523, 1999.

Carr DB, Cooper DC, Ulrich SL, Spruston N, Surmeier DJ. Serotonin receptor activation inhibits sodium current and dendritic excitability in prefrontal cortex via a protein kinase C-dependent mechanism. *J Neurosci* 22: 6846–6855, 2002.

Casada JH, Dafny N. Restraint and stimulation of bed nucleus of the stria terminalis produce similar stress-like behaviors. *Brain Res Bull* 27: 207–212, 1991.

Casada JH, Dafny N. Evidence for two different afferent pathways carrying stress-related information (noxious and amygdala stimulation) to the bed nucleus of the stria terminalis. *Brain Res* 579: 93–98, 1992.

Casada JH, Dafny N. Responses of neurons in bed nucleus of the stria terminalis to microiontophoretically applied morphine, norepinephrine and acetylcholine. *Neuropharmacology* 32: 279–284, 1993.

Catterall WA. Structure and regulation of voltage-gated Ca^{2+} channels. *Annu Rev Cell Dev Biol* 16: 521–555, 2000.

Chen S, Wang J, Siegelbaum SA. Properties of hyperpolarization-activated pacemaker current defined by coassembly of HCN1 and HCN2 subunits and basal modulation by cyclic nucleotide. *J Gen Physiol* 117: 491–504, 2001.

Crill WE. Persistent sodium current in mammalian central neurons. *Annu Rev Physiol* 58: 349–362, 1996.

Dalsass M, Siegel A. The bed nucleus of the stria terminalis: electrophysiological properties and responses to amygdaloid and hypothalamic stimulation. *Brain Res* 425: 346–350, 1987.

Dalsass M, Siegel A. Opioid peptide regulation of neurons in the bed nucleus of the stria terminalis: a microiontophoretic study. *Brain Res* 531: 346–349, 1990.

Dascal N, Schreibmayer W, Lim NF, Wang W, Chavkin C, DiMagno L, Labarca C, Kieffer BL, Gaveriaux-Ruff C, Trollinger D. Atrial G protein-activated K^+ channel: expression cloning and molecular properties. *Proc Natl Acad Sci USA* 90: 10235–10239, 1993.

Day M, Carr DB, Ulrich S, Ilijic E, Tkatch T, Surmeier DJ. Dendritic excitability of mouse frontal cortex pyramidal neurons is shaped by the interaction among HCN, Kir2, and Kleak channels. *J Neurosci* 25: 8776–8787, 2005.

De Jeu M, Geurtsen A, Pennartz C. A Ba(2+)-sensitive K(+) current contributes to the resting membrane potential of neurons in rat suprachiasmatic nucleus. *J Neurophysiol* 88: 869–878, 2002.

De Olmos JS, Alheid GF, Beltramino CA. Amygdala. In: *The Rat Nervous System: Forebrain and Midbrain*, edited by Paxinos G. New York: Academic Press, 1985, vol. 1, p. 223.

Dong HW, Petrovich GD, Swanson LW. Topography of projections from amygdala to bed nuclei of the stria terminalis. *Brain Res Brain Res Rev* 38: 192–246, 2001.

Dumont EC, Williams JT. Noradrenaline triggers $GABA_A$ inhibition of bed nucleus of the stria terminalis neurons projecting to the ventral tegmental area. *J Neurosci* 24: 8198–8204, 2004.

Egli RE, Kash TL, Choo K, Savchenko V, Matthews RT, Blakely RD, Winder DG. Norepinephrine modulates glutamatergic transmission in the bed nucleus of the stria terminalis. *Neuropsychopharmacology* 30: 657–668, 2005.

Egli RE, Winder DG. Dorsal and ventral distribution of excitable and synaptic properties of neurons of the bed nucleus of the stria terminalis. *J Neurophysiol* 90: 405–414, 2003.

Erb S, Stewart J. A role for the bed nucleus of the stria terminalis, but not the amygdala, in the effects of corticotropin-releasing factor on stress-induced reinstatement of cocaine seeking. *J Neurosci* 19: RC35, 1999.

Farley J, Auerbach S. Protein kinase C activation induces conductance changes in Hermissenda photoreceptors like those seen in associative learning. [Erratum appears in Nature 1986 Dec 18–31;324(6098):702]. *Nature* 319: 220–223, 1986.

Fisher R, Johnston D. Differential modulation of single voltage-gated calcium channels by cholinergic and adrenergic agonists in adult hippocampal neurons. *J Neurophysiol* 64: 1291–1302, 1990.

Franqueza L, Valenzuela C, Eck J, Tamkun MM, Tamargo J, Snyders DJ. Functional expression of an inactivating potassium channel (Kv4.3) in a mammalian cell line. *Cardiovasc Res* 41: 212–219, 1999.

Fraser DD, MacVicar BA. Low-threshold transient calcium current in rat hippocampal lacunosum-moleculare interneurons: kinetics and modulation by neurotransmitters. *J Neurosci* 11: 2812–2820, 1991.

Georges F, Aston-Jones G. Activation of ventral tegmental area cells by the bed nucleus of the stria terminalis: a novel excitatory amino acid input to midbrain dopamine neurons. *J Neurosci* 22: 5173–5187, 2002.

Goldin AL. Resurgence of sodium channel research. *Annu Rev Physiol* 63: 871–894, 2001.

Gorelova NA, Yang CR. Dopamine D1/D5 receptor activation modulates a persistent sodium current in rat prefrontal cortical neurons in vitro. *J Neurophysiol* 84: 75–87, 2000.

Gray TS, Magnuson DJ. Peptide immunoreactive neurons in the amygdala and the bed nucleus of the stria terminalis project to the midbrain central gray in the rat. *Peptides* 13: 451–460, 1992.

Gutman GA, Chandy KG, Grissmer S, Lazdunski M, McKinnon D, Pardo LA, Robertson GA, Rudy B, Sanguinetti MC, Stuhmer W, Wang X. International Union of Pharmacology. LIII. Nomenclature and molecular relationships of voltage-gated potassium channels. *Pharmacol Rev* 57: 473–508, 2005.

Hammack SE, Guo J, Hazra R, Rainnie DG. Subthreshold intrinsic membrane currents actively modulate the firing properties of neurons in the anterolateral group of the bed nucleus of the stria terminalis (BNST). *Proc Soc Neurosci*, Atlanta, GA, 2006.

Hammack SE, Haensly JW, Rainnie DG. Activation of 5-HT7 receptors mediates a depolarizing response in a subset of neurons in the anterolateral cell group of the bed nucleus of the stria terminalis. *Proc Soc Neurosci*, Washington, DC, 2005.

Hammack SE, Richey KJ, Watkins LR, Maier SF. Chemical lesion of the bed nucleus of the stria terminalis blocks the behavioral consequences of uncontrollable stress. *Behav Neurosci* 118: 443–448, 2004.

Hartmann HA, Colom LV, Sutherland ML, Noebels JL. Selective localization of cardiac SCN5A sodium channels in limbic regions of rat brain. *Nat Neurosci* 2: 593–595, 1999.

Harvey PJ, Li X, Li Y, Bennett DJ. 5-HT2 receptor activation facilitates a persistent sodium current and repetitive firing in spinal motoneurons of rats with and without chronic spinal cord injury. *J Neurophysiol* 96: 1158–1170, 2006.

Herbison AE, Pape JR, Simonian SX, Skynner MJ, Sim JA. Molecular and cellular properties of GnRH neurons revealed through transgenics in the mouse. *Mol Cell Endocrinol* 185: 185–194, 2001.

Ho K, Nichols CG, Lederer WJ, Lytton J, Vassilev PM, Kanazirska MV, Hebert SC. Cloning and expression of an inwardly rectifying ATP-regulated potassium channel. *Nature* 362: 31–38, 1993.

Hur EE, Zaborszky L. Vglut2 afferents to the medial prefrontal and primary somatosensory cortices: a combined retrograde tracing in situ hybridization. *J Comp Neurol* 483: 351–373, 2005.

Inanobe A, Fujita A, Ito M, Tomoike H, Inageda K, Kurachi Y. Inward rectifier K^+ channel Kir2.3 is localized at the postsynaptic membrane of excitatory synapses. *Am J Physiol Cell Physiol* 282: C1396–C1403, 2002.

Ingram CD, Cutler KL, Wakerley JB. Oxytocin excites neurones in the bed nucleus of the stria terminalis of the lactating rat in vitro. *Brain Res* 527: 167–170, 1990.

Isomoto S, Kondo C, Kurachi Y. Inwardly rectifying potassium channels: their molecular heterogeneity and function. *Jpn J Physiol* 47: 11–39, 1997.

Jasnow AM, Davis M, Huhman KL. Involvement of central amygdalar and bed nucleus of the stria terminalis corticotropin-releasing factor in behavioral responses to social defeat. *Behav Neurosci* 118: 1052–1061, 2004.

Ju G, Swanson LW, Simerly RB. Studies on the cellular architecture of the bed nuclei of the stria terminalis in the rat: II. Chemoarchitecture. *J Comp Neurol* 280: 603–621, 1989.

Kaneda M, Kaneko A. Voltage-gated sodium currents in isolated retinal ganglion cells of the cat: relation between the inactivation kinetics and the cell type. *Neurosci Res* 11: 261–275, 1991.

Karschin C, Dissmann E, Stuhmer W, Karschin A. IRK(1–3) and GIRK(1–4) inwardly rectifying K^+ channel mRNAs are differentially expressed in the adult rat brain. *J Neurosci* 16: 3559–3570, 1996.

Klockner U, Lee JH, Cribbs LL, Daud A, Hescheler J, Pereverzev A, Perez-Reyes E, Schneider T. Comparison of the Ca2+ currents induced by expression of three cloned alpha1 subunits, alpha1G, alpha1H and alpha1I, of low-voltage-activated T-type Ca2+ channels. *Eur J Neurosci* 11: 4171–4178, 1999.

Larriva-Sahd J. Juxtacapsular nucleus of the stria terminalis of the adult rat: extrinsic inputs, cell types, and neuronal modules: a combined Golgi and electron microscopic study. *J Comp Neurol* 475: 220–237, 2004.

Larriva-Sahd J. Histological and cytological study of the bed nuclei of the stria terminalis in adult rat. II. Oval nucleus: extrinsic inputs, cell types, neuropil, and neuronal modules. *J Comp Neurol* 497: 772–807, 2006.

Lechner SM, Valentino RJ. Glucocorticoid receptor-immunoreactivity in corticotrophin-releasing factor afferents to the locus coeruleus. *Brain Res* 816: 17–28, 1999.

Lee JH, Gomora JC, Cribbs LL, Perez-Reyes E. Nickel block of three cloned T-type calcium channels: low concentrations selectively block alpha1H. *Biophys J* 77: 3034–3042, 1999.

Lenglet S, Louiset E, Delarue C, Vaudry H, Contesse V. Activation of 5-HT(7) receptor in rat glomerulosa cells is associated with an increase in adenylyl cyclase activity and calcium influx through T-type calcium channels. *Endocrinology* 143: 1748–1760, 2002.

Levita L, Hammack SE, Mania I, Li XY, Davis M, Rainnie DG. 5-Hydroxytryptamine1A-like receptor activation in the bed nucleus of the stria terminalis: electrophysiological and behavioral studies. *Neuroscience* 128: 583–596, 2004.

Llinas RR, Steriade M. Bursting of thalamic neurons and states of vigilance. *J Neurophysiol* 95: 3297–3308, 2006.

Locke RE, Nerbonne JM. Three kinetically distinct Ca^{2+}-independent depolarization-activated K^+ currents in callosal-projecting rat visual cortical neurons. *J Neurophysiol* 78: 2309–2320, 1997.

Ludwig A, Zong X, Jeglitsch M, Hofmann F, Biel M. A family of hyperpolarization-activated mammalian cation channels. *Nature* 393: 587–591, 1998.

Marchetti C, Carbone E, Lux HD. Effects of dopamine and noradrenaline on Ca channels of cultured sensory and sympathetic neurons of chick. *Pflügers Arch/Eur J Physiol* 406: 104–111, 1986.

Martina M, Royer S, Paré D. Physiological properties of central medial and central lateral amygdala neurons. *J Neurophysiol* 82: 1843–1854, 1999.

Maurice N, Tkatch T, Meisler M, Sprunger LK, Surmeier DJ. D1/D5 dopamine receptor activation differentially modulates rapidly inactivating and persistent sodium currents in prefrontal cortex pyramidal neurons. *J Neurosci* 21: 2268–2277, 2001.

McCormick DA, Pape HC. Properties of a hyperpolarization-activated cation current and its role in rhythmic oscillation in thalamic relay neurones. *J Physiol* 431: 291–318, 1990.

McDonald AJ. Neurons of the bed nucleus of the stria terminalis: a Golgi study in the rat. *Brain Res Bull* 10: 111–120, 1983.

Mistrik P, Mader R, Michalakis S, Weidinger M, Pfeifer A, Biel M. The murine HCN3 gene encodes a hyperpolarization-activated cation channel with slow kinetics and unique response to cyclic nucleotides. *J Biol Chem* 280: 27056–27061, 2005.

Monteggia LM, Eisch AJ, Tang MD, Kaczmarek LK, Nestler EJ. Cloning and localization of the hyperpolarization-activated cyclic nucleotide-gated channel family in rat brain. *Brain Res Mol Brain Res* 81: 129–139, 2000.

Morris NP, Fyffe RE, Robertson B. Characterisation of hyperpolarization-activated currents (I(h)) in the medial septum/diagonal band complex in the mouse. *Brain Res* 1006: 74–86, 2004.

Nakajima Y, Nakajima S, Leonard RJ, Yamaguchi K. Acetylcholine raises excitability by inhibiting the fast transient potassium current in cultured hippocampal neurons. *Proc Natl Acad Sci USA* 83: 3022–3026, 1986.

Nelson S. Cortical microcircuits: diverse or canonical? *Neuron* 36: 19–27, 2002.

Newman SW. The medial extended amygdala in male reproductive behavior. A node in the mammalian social behavior network. *Ann NY Acad Sci* 877: 242–257, 1999.

Nichols CG, Lopatin AN. Inward rectifier potassium channels. *Annu Rev Physiol* 59: 171–191, 1997.

Nisenbaum ES, Wilson CJ. Potassium currents responsible for inward and outward rectification in rat neostriatal spiny projection neurons. *J Neurosci* 15: 4449–4463, 1995.

Perez-Reyes E. Molecular physiology of low-voltage-activated T-type calcium channels. *Physiol Rev* 83: 117–161, 2003.

Peruzzi D, Sivaramakrishnan S, Oliver DL. Identification of cell types in brain slices of the inferior colliculus. *Neuroscience* 101: 403–416, 2000.

Placantonakis DG, Schwarz C, Welsh JP. Serotonin suppresses subthreshold and suprathreshold oscillatory activity of rat inferior olivary neurones in vitro. *J Physiol* 524: 833–851, 2000.

Qiu DL, Chu CP, Shirasaka T, Tsukino H, Nakao H, Kato K, Kunitake T, Katoh T, Kannan H. Corticotrophin-releasing factor augments the *I*(H) in rat hypothalamic paraventricular nucleus parvocellular neurons in vitro. *J Neurophysiol* 94: 226–234, 2005.

Qiu J, Bosch MA, Jamali K, Xue C, Kelly MJ, Ronnekleiv OK. Estrogen upregulates T-type calcium channels in the hypothalamus and pituitary. *J Neurosci* 26: 11072–11082, 2006.

Rainnie DG. Neurons of the bed nucleus of the stria terminalis (BNST). Electrophysiological properties and their response to serotonin. *Ann NY Acad Sci* 877: 695–699, 1999.

Rainnie DG, Bergeron R, Sajdyk TJ, Patil M, Gehlert DR, Shekhar A. Corticotrophin releasing factor-induced synaptic plasticity in the amygdala translates stress into emotional disorders. *J Neurosci* 24: 3471–3479, 2004.

Roberts L, Greene JR. Hyperpolarization-activated current (Ih): a characterization of subicular neurons in brain slices from socially and individually housed rats. *Brain Res* 1040: 1–13, 2005.

Robertson B. The real life of voltage-gated K^+ channels: more than model behaviour. *Trends Pharmacol Sci* 18: 474–483, 1997.

Robinson RB, Siegelbaum SA. Hyperpolarization-activated cation currents: from molecules to physiological function. *Annu Rev Physiol* 65: 453–480, 2003.

Rudy B. Diversity and ubiquity of K channels. *Neuroscience* 25: 729–749, 1988.

Ryu PD, Randic M. Low- and high-voltage-activated calcium currents in rat spinal dorsal horn neurons. *J Neurophysiol* 63: 273–285, 1990.

Santoro B, Chen S, Luthi A, Pavlidis P, Shumyatsky GP, Tibbs GR, Siegelbaum SA. Molecular and functional heterogeneity of hyperpolarization-activated pacemaker channels in the mouse CNS. *J Neurosci* 20: 5264–5275, 2000.

Santoro B, Liu DT, Yao H, Bartsch D, Kandel ER, Siegelbaum SA, Tibbs GR. Identification of a gene encoding a hyperpolarization-activated pacemaker channel of brain. *Cell* 93: 717–729, 1998.

Saraga F, Skinner FK. Dynamics and diversity in interneurons: a model exploration with slowly inactivating potassium currents. *Neuroscience* 113: 193–203, 2002.

Serodio P, Rudy B. Differential expression of Kv4 K^+ channel subunits mediating subthreshold transient K^+ (A-type) currents in rat brain. *J Neurophysiol* 79: 1081–1091, 1998.

Shimada S, Inagaki S, Kubota Y, Ogawa N, Shibasaki T, Takagi H. Coexistence of peptides (corticotropin releasing factor/neurotensin and substance P/somatostatin) in the bed nucleus of the stria terminalis and central amygdaloid nucleus of the rat. *Neuroscience* 30: 377–383, 1989.

Song WJ. Genes responsible for native depolarization-activated K^+ currents in neurons. *Neurosci Res* 42: 7–14, 2002.

Stafstrom CE, Schwindt PC, Chubb MC, Crill WE. Properties of persistent sodium conductance and calcium conductance of layer V neurons from cat sensorimotor cortex in vitro. *J Neurophysiol* 53: 153–170, 1985.

Stanfield PR, Davies NW, Shelton PA, Khan IA, Brammar WJ, Standen NB, Conley EC. The intrinsic gating of inward rectifier K^+ channels

expressed from the murine IRK1 gene depends on voltage, K^+ and Mg^{2+}. *J Physiol* 475: 1–7, 1994.

Sun N, Cassell MD. Intrinsic GABAergic neurons in the rat central extended amygdala. *J Comp Neurol* 330: 381–404, 1993.

Takigawa T, Alzheimer C. Phasic and tonic attenuation of EPSPs by inward rectifier K^+ channels in rat hippocampal pyramidal cells. *J Physiol* 539: 67–75, 2002.

Talley EM, Cribbs LL, Lee JH, Daud A, Perez-Reyes E, Bayliss DA. Differential distribution of three members of a gene family encoding low voltage-activated (T-type) calcium channels. *J Neurosci* 19: 1895–1911, 1999.

Tsaur ML, Chou CC, Shih YH, Wang HL. Cloning, expression and CNS distribution of Kv4.3, an A-type K^+ channel alpha subunit. *FEBS Lett* 400: 215–220, 1997.

Urbani A, Belluzzi O. Riluzole inhibits the persistent sodium current in mammalian CNS neurons. *Eur J Neurosci* 12: 3567–3574, 2000.

Varga AW, Yuan LL, Anderson AE, Schrader LA, Wu GY, Gatchel JR, Johnston D, Sweatt JD. Calcium-calmodulin-dependent kinase II modulates Kv4.2 channel expression and upregulates neuronal A-type potassium currents. *J Neurosci* 24: 3643–3654, 2004.

Vega-Saenz de Miera EC, Rudy B, Sugimori M, Llinas R. Molecular characterization of the sodium channel subunits expressed in mammalian cerebellar Purkinje cells. *Proc Natl Acad Sci USA* 94: 7059–7064, 1997.

Veinante P, Stoeckel ME, Freund-Mercier MJ. GABA- and peptide-immunoreactivities co-localize in the rat central extended amygdala. *Neuroreport* 8: 2985–2989, 1997.

Walker DL, Davis M. Double dissociation between the involvement of the bed nucleus of the stria terminalis and the central nucleus of the amygdala in startle increases produced by conditioned versus unconditioned fear. *J Neurosci* 17: 9375–9383, 1997.

Walker DL, Toufexis DJ, Davis M. Role of the bed nucleus of the stria terminalis versus the amygdala in fear, stress, and anxiety. *Eur J Pharmacol* 463: 199–216, 2003.

Wang WT, Wan YH, Zhu JL, Lei GS, Wang YY, Zhang P, Hu SJ. Theta-frequency membrane resonance and its ionic mechanisms in rat subicular pyramidal neurons. *Neuroscience* 140: 45–55, 2006.

Woodhams PL, Roberts GW, Polak JM, Crow TJ. Distribution of neuropeptides in the limbic system of the rat: the bed nucleus of the stria terminalis, septum and preoptic area. *Neuroscience* 8: 677–703, 1983.

Wu J, Hablitz JJ. Cooperative activation of D1 and D2 dopamine receptors enhances a hyperpolarization-activated inward current in layer I interneurons. *J Neurosci* 25: 6322–6328, 2005.

Wu N, Enomoto A, Tanaka S, Hsiao CF, Nykamp DQ, Izhikevich E, Chandler SH. Persistent sodium currents in mesencephalic v neurons participate in burst generation and control of membrane excitability. *J Neurophysiol* 93: 2710–2722, 2005.